EUROPEAN ORGANIZATION FOR NUCLEAR RESEARCH

MEASUREMENT AND ANALYSIS OF THE REACTION $\pi^- p \to \rho^0 n$ ON A POLARIZED TARGET

(CERN-Munich Collaboration)

H. Becker*), G. Blanar, W. Blum, M. Cerrada, H. Dietl, J. Gallivan,
B. Gottschalk**), G. Grayer***), G. Hentschel†), E. Lorenz,
G. Lütjens, G. Lutz, W. Männer, D. Notz††), R. Richter,
U. Stierlin and B. Stringfellow×)

Max Planck Institute, Munich, Germany

V. Chabaud, B. Hyams and T. Papadopoulou××)

CERN, Geneva, Switzerland

J. de Groot×××)

Zeeman Laboratory, Amsterdam, The Netherlands

B. Niczyporuk, K. Rybicki, M. Turala and A. Zalewska

Institute of Nuclear Physics, Cracow, Poland

Geneva - 29 September 1978

(Submitted to Nuclear Physics B)

---

*) Now at Technische Fachhochschule, Saarbrücken, Germany.
**) Visitor from Northeastern University, Boston, Mass., USA.
***) Now at Rutherford Laboratory, Chilton, Didcot, Oxon., England.
†) Now at the University of Frankfurt, Germany.
††) Now at DESY, Hamburg, Germany.
×) Now at the Nuclear Research Centre, Strasbourg, France.
××) Now at the National Technical University, Athens, Greece.
×××) Now at CERN, Geneva, Switzerland.

ABSTRACT

The reaction $\pi^- p \to \pi^+ \pi^- n$ has been measured in a high-statistics experiment on a transversely polarized proton target at 17.2 GeV, and unexpectedly large nucleon polarization effects have been observed. Combining the results of this experiment with a measurement on a hydrogen target allows a model-independent partial wave analysis in terms of the "nucleon transversity" amplitudes. Unique or at most twofold ambiguous solutions are obtained. In particular we find a high lower limit ($\gtrsim$ 30%) of the spin non-flip unnatural exchange amplitudes at low $|t|$. These amplitudes, interpreted as being due to the exchange of an object with the quantum numbers of the A_1, have been assumed to be absent in previous analyses. In checking the consequences of this finding on the old results, we test the validity of the rank-two assumptions for the density matrix. We find a small but significant deviation, which shows the need for a new phase-shift analysis including the A_1 exchange contribution.

1. INTRODUCTION

The reaction $\pi^- p \to \pi^+ \pi^- n$ has been measured in high-statistics experiments on hydrogen targets [1,2]. Data from ref. [1], henceforth called experiment I, have been used for a study of $\pi\pi$ scattering [3-5,19] and for the study of resonance production [6,7]. Phenomenological assumptions had to be introduced as no nucleon polarization measurements existed at that time; in particular the absence of A_1-type exchange was assumed in all these analyses. By this we mean that s-channel helicity amplitudes were supposed to be of a purely spin-flip type for the unnatural parity exchange.

In the present experiment (hereafter called experiment II) we measured the same reaction on a transversely polarized target in order to test these assumptions and, more generally, to allow a model-independent amplitude determination for this reaction. Strong nucleon polarization effects were observed even at low four-momentum transfer. This clearly demonstrates the presence of amplitudes corresponding to the exchange of an object with the quantum numbers of the A_1. The data from this experiment taken together with results from experiment I allow a model-independent determination of the "nucleon transversity" amplitudes. Although the information is not sufficient to determine nucleon helicity flip and non-flip amplitudes, lower limits for the A_1-type exchange amplitudes are obtained. The presence of this exchange has consequences for the old $\pi\pi$ phase-shift analyses.

Preliminary results of this experiment have been reported at the Tbilisi Conference [8] and at the Argonne Symposium on Polarized Beams and Targets [9]. A description of the experiment, including details of the apparatus and the apparatus-dependent aspects of the analysis, can be found in ref. [10], while the formalism and the method of amplitude analysis for a transversely polarized target are described in ref. [11]. The higher mass region is covered in another paper [12].

2. DEFINITIONS, MOMENTS, AND AMPLITUDES

At fixed beam momentum the reaction is completely determined by five variables for which we choose (fig. 1) $m_{\pi\pi}$ the mass of the pion pair, t the square of the

four-momentum transfer to the nucleon, ψ the angle between the normal to the reaction plane and the (transverse) proton polarization P, and θ, ϕ the decay angles of the π^- in the $\pi^+\pi^-$ rest frame.

Owing to parity conservation and spin ½ of the nucleon, the angular distribution at fixed s is of the form

$$I(m_{\pi\pi},t,\psi,\theta,\phi) = I_0(m_{\pi\pi},t,\theta,\phi) + P\cos\psi\, I_1(m_{\pi\pi},t,\theta,\phi) + P\sin\psi\, I_2(m_{\pi\pi},t,\theta,\phi)$$

$$= \sum_{L,M} t_M^L(m_{\pi\pi},t)\ \mathrm{Re}\ Y_M^L(\cos\theta,\phi) + P\cos\psi \sum_{L,M} p_M^L(m_{\pi\pi},t)\ \mathrm{Re}\ Y_M^L(\cos\theta,\phi)$$

$$+ P\sin\psi \sum_{L,M} r_M^L(m_{\pi\pi},t)\ \mathrm{Im}\ Y_M^L(\cos\theta,\phi)\ ,$$

with I_0, I_1 symmetric and I_2 antisymmetric in ϕ. Consequently the result of the experiment can be represented by the $m_{\pi\pi}$- and t-dependence of the moments:

$$t_M^L = \varepsilon_M\langle \mathrm{Re}\ Y_M^L\rangle = \varepsilon_M \frac{1}{2\pi}\int \mathrm{Re}\ Y_M^L(\Omega)\ I(\psi,\Omega)\ d\Omega\ d\psi$$

$$p_M^L = 2\varepsilon_M\langle\cos\psi\ \mathrm{Re}\ Y_M^L\rangle = 2\varepsilon_M \frac{1}{2\pi}\int \cos\psi\ \mathrm{Re}\ Y_M^L(\Omega)\ I(\psi,\Omega)\ d\Omega\ d\psi$$

$$r_M^L = 4\langle\sin\psi\ \mathrm{Im}\ Y_M^L\rangle = 4\,\frac{1}{2\pi}\int \sin\psi\ \mathrm{Im}\ Y_M^L(\Omega)\ I(\psi,\Omega)\ d\Omega\ d\psi\ ,$$

$$(\varepsilon_{M=0} = 1,\ \varepsilon_{M\neq 0} = 2)\ .$$

A complete description of the reaction is given by the set of $m_{\pi\pi}$ and t-dependent helicity amplitudes $\langle jm\chi|T|\lambda\rangle$, where j, m are the spin and helicity of the π pair, λ and χ the helicities of proton and neutron

$$N_m^j = \langle j,m,\tfrac{1}{2}|T|\tfrac{1}{2}\rangle = (-1)^{m+1}\langle j,-m,-\tfrac{1}{2}|T|-\tfrac{1}{2}\rangle$$

$$F_m^j = \langle j,m,\tfrac{1}{2}|T|-\tfrac{1}{2}\rangle = (-1)^{m}\langle j,-m,-\tfrac{1}{2}|T|\tfrac{1}{2}\rangle\ .$$

Alternatively one uses combinations of amplitudes corresponding to unnatural (U) and natural (N) spin-parity exchange [13]:

$$^{U}n_0^j = N_0^j$$

$$^{U}n_m^j = \frac{1}{\sqrt{2}}\left[N_m^j + (-1)^m N_{-m}^j\right] \qquad \text{for } m \neq 0$$

$$^{N}n_m^j = \frac{1}{\sqrt{2}}\left[N_m^j - (-1)^m N_{-m}^j\right] .$$

Analogous equations hold for spin-flip amplitudes replacing n by f and N by F.

We will deal mainly with two sets of nucleon transversity amplitudes g and h, which correspond to neutron polarization perpendicular to the reaction plane:

$$^{U}g_m^j = \frac{1}{\sqrt{2}}\left(^{U}n_m^j + i\ ^{U}f_m^j\right), \qquad ^{N}g_m^j = \frac{1}{\sqrt{2}}\left(^{N}n_m^j - i\ ^{N}f_m^j\right),$$

$$^{U}h_m^j = \frac{1}{\sqrt{2}}\left(^{U}n_m^j - i\ ^{U}f_m^j\right), \qquad ^{N}h_m^j = \frac{1}{\sqrt{2}}\left(^{N}n_m^j + i\ ^{N}f_m^j\right).$$

(Further on we use the shortened notation $g_S = {}^{U}g_0^0$, $g_0 = {}^{U}g_0^1$, $g_U = {}^{U}g_1^1$, $g_N = {}^{N}g_1^1$, etc.). Note that we normalize the amplitudes in such a way that the sum of their squares gives the differential cross-section $d^2\sigma/dm_{\pi\pi}dt$. This is seen in table 1 where the moments of the angular distributions are given in terms of amplitudes for the case of S- and P-waves only. It is valid for both s- or t-channel moments as long as the $\pi\pi$ helicities in the amplitudes are chosen according to the given channel, and the nucleon helicities are defined in the s-channel.

Table 1 also shows the motivation for introducing nucleon transversity amplitudes. No products between g and h amplitudes appear; consequently the phase between the set of g and the set of h amplitudes cannot be measured in this experiment in which the neutron polarization is not observed. Therefore the theoretically more interesting n and f amplitudes cannot be determined in a model-independent way. We mention that these properties hold for arbitrary $\pi\pi$ spin and that an experiment with a longitudinally polarized target would not alter this situation.

Nevertheless we can still determine everything (in principle) within each set of the nucleon transversity amplitudes g or h.

3. EXPERIMENTAL SET-UP

The experiment was done with the CERN-Munich spectrometer (fig. 2) at the CERN Proton Synchrotron (PS) with incident π^- of 17.2 GeV. A butanol target T [14] (length = 10 cm, $\emptyset$ = 20 mm, average polarization 68%) inside a 25 kG homogeneous field was used. A small sample of data was taken with a hydrogen target of identical shape instead of the butanol target, and using the same cryostat. A tungsten-scintillator shower counter system (F) between the pole faces of the target magnet suppressed background from events with additional π^0's or charged particles. Multiwire proportional chambers (MWPC) directly in front of and behind the target in the magnetic field allowed a good vertex determination.

The rest of the spectrometer as well as the trigger was essentially identical to that of experiment I. The beam pions are identified by the threshold Čerenkov counter C_1 and measured with the beam spectrometer consisting of two 2 m bending magnets (M) between four packs of magnetostrictive spark chambers (SCh). The charged secondary particles are momentum-analysed using the spectrometer magnet (AEG) and spark chambers before and after the magnet. The particles are identified by two multicell Čerenkov counters (C_2 and C_3); C_2 was filled with CO_2 at atmospheric pressure (threshold for pions 4.7 GeV, for kaons 16.7 GeV), C_3 with neopentane. A double array of 10 cm wide vertical counters (E and G) was used to define the charged multiplicity of the event. Coincidences between corresponding elements of these two counters were required to suppress random noise and δ-electron background.

In the trigger, we required a beam pion defined by signals from the scintillation counters $B_1B_2B_3\bar{B}_4$ and C_1, an interaction signalled by a hit in a scintillation counter I which had a hole at the position of the beam, no signal in the veto counters F and H, multiplicity two in the EG array, and no hit in the beam veto counter D.

4. EVENT RECONSTRUCTION AND ACCEPTANCE CORRECTIONS

A total of about 2×10^7 triggers were recorded on tape. These events were processed by a geometrical reconstruction program. The principal parts of this program were: track finding in all spectrometer sections equipped with spark chambers, track matching in the spectrometer magnet, and forming a vertex with a beam track in the target inside the magnetic field. Only events with two secondaries of opposite charge were accepted. The program needed about 20 ms CDC 7600 time for the processing of a single trigger. Then we distinguished secondary pions from kaons and protons by demanding that at least one of them gave a signal in C_2. The missing mass (MM) cut was $MM^2 < 1.4\ GeV^2$. Applying all these criteria, we are left with 1.2×10^6 events off butanol, about one third of these corresponding to collisions with free protons (hydrogen atoms in the butanol molecule).

In addition to these butanol data, we recorded data taken under identical conditions on a pure hydrogen target as well as various other calibration data. After all cuts we were left with 34×10^3 hydrogen events.

The presence of carbon and oxygen in butanol (C_4H_9OH) leads to some problems in experiment II, where the outgoing neutron remains undetected and an individual separation of events off hydrogen from those produced on complex nuclei -- as done in elastic scattering where one has four constraints -- is not possible. (The widening of the missing-mass distribution due to the neglect of the Fermi motion in the calculation is negligible compared to the missing-mass resolution.) As a consequence we can only extract from this experiment the polarization-dependent part of the cross-section $d^2\sigma/dm_{\pi\pi}dt\ \langle \cos\psi\ \mathrm{Re}\ Y_M^L \rangle$ and $d^2\sigma/dm_{\pi\pi}dt\ \langle \sin\psi\ \mathrm{Im}\ Y_M^L \rangle$ as the unpolarized carbon and oxygen do not contribute to it. For the amplitude analysis the result of this experiment is combined with that of experiment I taken at the same beam momentum of 17.2 GeV. Thus all polarization-independent moments $\langle \mathrm{Re}\ Y_M^L \rangle$ shown throughout the paper (with the exception of fig. 5) are from experiment I.

For a determination of the moments, corrections had to be applied for the geometrical acceptance as well as for various other geometrical configuration-dependent

losses. The latter were corrected by attributing weights (average value $\bar{w}$) to the events: neutron interaction in the veto counters $\bar{w} = 1.4$, δ-rays firing veto counters $\bar{w} = 1.16$, secondary interactions in the target $\bar{w} = 1.05$, and π decays $\bar{w} = 1.03$.

The acceptance correction was performed by two different methods, one being a generalization [10] of the method of moments, the other a generalization of the χ^2 method, both described in ref. 1. In the latter method the number of observed events in a given $\cos\theta$, ϕ bin as well as the $\cos\psi$ and $\sin\psi$ moments were fitted by the product of assumed produced events distribution and the acceptance of the apparatus. In calculating the χ^2 for each $\cos\theta$, ϕ bin, the correlation in the errors of events and moments was taken into account. Both methods gave consistent results; those presented in this paper were obtained using the first method. We restricted the moments to $L \leq 2$, thereby neglecting the small D-wave in the analysis (6% of intensity at the highest mass considered).

We emphasize that the moments $\langle \cos\psi \ \mathrm{Re}\ Y_M^L \rangle$ and $\langle \sin\psi \ \mathrm{Im}\ Y_M^L \rangle$ could be obtained with one single target polarization direction only, since our apparatus covers a large solid angle -- the acceptance for isotropic decay varies between 80% and 40% in the mass and t-range covered in this paper. In order to minimize systematic errors, the polarization direction of the target was reversed once a day (by changing the klystron frequency slightly, leaving the spectrometer and therefore its acceptance unchanged). The data for the two polarization directions were analysed separately and the results -- which were consistent within statistics -- averaged.

5. RAW DATA SPECTRA

The missing-mass spectrum of events from butanol (calculated under the assumption that the process occurs on hydrogen at rest) shows a significant enhancement in the MM^2 above the mass of the neutron (fig. 3). This enhancement is not seen in the data taken under identical conditions on the hydrogen target, which show an almost symmetric distribution around the neutron peak. The background at high MM^2 is independent of $m_{\pi\pi}$ but varies with t and is strongest for small t. It is most

probably due to complex interactions on carbon and oxygen in which the excited nuclei decay in a mode not detected by our veto counter system, e.g. by emitting two neutrons.

Strong nucleon polarization effects are already seen in the data before correcting for the acceptance of the apparatus when we compare distributions of events where the only change is the proton polarization direction -- the apparatus, including magnet fields, was otherwise identical. The change with proton polarization of the distribution in the angle ψ between the normal to the production plane and the *positive* polarization direction (fig. 1), for events with $MM^2 < 1.4$ GeV^2, is shown in fig. 4. From the difference of the distributions, we conclude that for upward-pointing proton spin, the $\pi\pi$ resonance goes preferably to the right.

By multiplying the MM^2 distribution off butanol with this left-right asymmetry we can now single out a contribution which is due to events on hydrogen only (fig. 3). A perfectly symmetric peak around the neutron shows that the large mass tail is indeed due to events on complex nuclei. From this distribution we conclude that the background of events with recoiling N^*'s in our polarization-dependent moments is below 1%.

6. CROSS-SECTION AND ANGULAR DISTRIBUTION

As already mentioned, in this experiment we measure only the polarization-dependent moments, since the polarization-independent moments $\langle \mathrm{Re}\ Y_M^L \rangle$ contain mostly events produced on complex nuclei. Nevertheless, it is interesting to note that the mass dependence of the angular distribution on butanol (fig. 5) is indistinguishable from that on pure hydrogen of experiment I (fig. 6a). This is also true for the t-dependence, with the exception of the very low-t region ($|t| < 0.02$ GeV^2/c^2) where we encounter also the strong background giving rise to the high-mass tail in the MM^2 distribution.

When combining the polarization-independent part of the cross-section $d^2\sigma/dm_{\pi\pi}dt\ \langle \mathrm{Re}\ Y_M^L \rangle$ from experiment I with the polarization-dependent part $d^2\sigma/dm_{\pi\pi}dt\ \langle \cos\psi\ \mathrm{Re}\ Y_M^L \rangle$ and $d^2\sigma/dm_{\pi\pi}dt\ \langle \sin\psi\ \mathrm{Im}\ Y_M^L \rangle$, we scale the latter to 100%

polarized protons. The results presented in the following correspond to a fictitious single experiment on 100% polarized pure protons. The statistical errors on the polarization-independent moments are those of a sample with 300,000 events; those of the polarization-dependent moments correspond to a sample of 60,000 events. There remains an uncertainty of 15% in the relative normalization of the two experiments and therefore in all normalized moments $\langle \cos\psi \ \mathrm{Re}\ Y_M^L \rangle$ and $\langle \sin\psi \ \mathrm{Im}\ Y_M^L \rangle$.

The cross-section t-dependence and normalized t-channel moments are shown in figs. 7 for the $\pi^+\pi^-$ mass range around the ρ meson ($0.71 < m_{\pi\pi} < 0.83$ GeV/c^2). The mass dependence for $0.005 < |t| < 0.2$ GeV^2/c^2 is seen in figs. 6.

A most interesting observation is the presence of strong polarization effects even in the low-t region. The left-right asymmetry defined by $2\langle \cos\psi \ Y_0^0 \rangle / \langle Y_0^0 \rangle$ is -0.5 in the low-t region, on a scale where the maximum value is one. This is very surprising since according to general belief this region should be dominated by one-pion exchange and should therefore show little or no polarization effect.

As seen in table 1 the $\langle \cos\psi \ \mathrm{Re}\ Y_M^L \rangle$ moments require the simultaneous presence of spin-flip and spin-non-flip amplitudes of equal naturality. In particular, the moments $\langle \cos\psi \ Y_0^1 \rangle$, $\langle \cos\psi \ \mathrm{Re}\ Y_1^1 \rangle$, and $\langle \cos\psi \ \mathrm{Re}\ Y_1^2 \rangle$ have only unnatural parity contributions. The presence of strong polarization-dependent moments therefore points to an appreciable magnitude of s-channel nucleon spin-non-flip amplitudes for unnatural parity exchange. These amplitudes are usually interpreted as corresponding to A_1 exchange.

The $\langle \sin\psi \ \mathrm{Im}\ Y_M^L \rangle$ moments are also given by the interference of flip and non-flip amplitudes but with different naturality. They are significant in the medium t-range where both unnatural parity (π and A_1) and natural parity (A_2) exchanges are present simultaneously.

7. AMPLITUDE ANALYSIS

For the case of S and P waves only, the system of equations (table 1) connecting nucleon transversity (g and h) amplitudes can be solved analytically. Fifteen

measured moments determine the 14 unknowns (8 moduli of amplitudes and 6 relative phases).

Suitable addition or subtraction leads to the following set of equations:

$$|g_S|^2 + 3|g_0|^2 = \sqrt{\pi}\left[(t_0^0 + p_0^0) + \sqrt{5}(t_0^2 + p_0^2)\right] = C_1$$

$$|g_0|^2 - |g_U|^2 = \frac{\sqrt{5\pi}}{2}\left[(t_0^2 + p_0^2) - \frac{1}{\sqrt{6}}(t_2^2 + p_2^2)\right] = C_2$$

$$|g_0||g_S| \cos \gamma_{S0} = \frac{1}{2}\sqrt{\pi}(t_0^1 + p_0^1) = C_3$$

$$|g_U||g_S| \cos \gamma_{US} = \frac{1}{2}\sqrt{\frac{\pi}{2}}(t_1^1 + p_1^1) = C_4$$

$$|g_U||g_0| \cos \gamma_{U0} = \frac{1}{2}\sqrt{\frac{5\pi}{6}}(t_1^2 + p_1^2) = C_5 \ .$$

Substituting for the relative phase $\gamma_{US} = \gamma_{U0} - \gamma_{S0}$, the set of equations can be transformed into a cubic equation [15] for $z = |g_0|^2$:

$$3z^3 - (C_1 + 3C_2)z^2 + (C_1C_2 + C_4^2 + C_3^2 - 3C_5^2)z + (C_1C_5^2 - 2C_3C_4C_5 - C_2C_3^2) = 0 \ .$$

In general we would obtain three solutions, but one of the solutions is unphysical. This is because of inequality relations for the coefficients C_i. We therefore obtain two sets of ambiguous solutions for $|g_S|$, $|g_0|$, $|g_U|$ and their relative phases. For the h amplitudes and their relative phases χ, an analogous set of equations can be found, again leading to two ambiguous solutions. Using the further relations

$$|g_U|^2 - |h_N|^2 = \sqrt{\frac{5\pi}{6}}(t_2^2 + p_2^2)$$

$$|h_U|^2 - |g_N|^2 = \sqrt{\frac{5\pi}{6}}(t_2^2 - p_2^2) \ ,$$

the remaining moduli are determined unambiguously and we are left with the last three equations in table 1 to determine the two remaining phases γ_{N0} and χ_{N0}:

$$|g_N||g_S| \cos(\gamma_{N0} - \gamma_{S0}) - |h_N||h_S| \cos(\chi_{N0} - \chi_{S0}) = -\sqrt{\frac{\pi}{2}}\, r_1^1$$

$$|g_N||g_0| \cos \gamma_{N0} - |h_N||h_0| \cos \chi_{N0} = -\sqrt{\frac{5\pi}{6}}\, r_1^2$$

$$|g_N||g_U| \cos(\gamma_{N0} - \gamma_{U0}) - |h_N||h_U| \cos(\chi_{N0} - \chi_{U0}) = -\sqrt{\frac{5\pi}{6}}\, r_2^2 \ .$$

Elimination of $\sin \chi_{N0}$ by combining the first and third equations and inserting $\cos \chi_{N0}$ from the second equation leads to an equation of the form

$$\sin(\gamma_{N0} + \alpha) = d \cos \alpha \ ,$$

with α and d expressed by previously determined quantities. With this additional twofold ambiguity, one arrives at a maximum of eight ambiguous solutions. In this counting we did not include the ambiguities arising from the possibility of changing the sign of all γ or all χ phases separately, or both simultaneously.

The analytic solutions were taken as starting values for a χ^2 minimization, fitting the measured moments by those calculated from the amplitudes according to the formulae in table 1. We also looked for additional ambiguous solutions by doing random searches for starting values of the χ^2 minimization. On the other hand, we did not use the results of the fit from one bin as an input to the neighbour, thus keeping a completely energy-independent approach. It turned out that the phases between natural and unnatural amplitudes γ_{N0} and χ_{N0} which are constrained only by the three $\langle \sin \psi \ \mathrm{Im}\ Y_M^L \rangle$ moments are badly determined by the experiment. Therefore we chose to consider solutions as being identical if they differed only in these two angles, which were anyway determined with large statistical errors. Similarly the sign of the other angles was not always well determined as only their cosine appears in the relevant equations. We therefore chose to present only the cosines of the angles between the unnatural parity exchange amplitudes.

The results of the amplitude analysis are shown in figs. 8 to 11. In general we find unique or at most twofold ambiguous solutions. If ambiguous solutions are found, we use the symbol ϕ for the "phase coherent solution", which is compatible with $\cos \gamma_{U0} = \cos \chi_{U0} = -1$, while ϕ is used for the other one.

The t-dependence of the moduli of the amplitudes is shown in fig. 8 for the $\pi^+\pi^-$ invariant mass range between 0.71 and 0.83 GeV spanning the ρ mass. Here we have normalized them so that their squares add up to unity. The cosines of the phases between the unnatural amplitudes are presented in fig. 9. The dependence on the $m_{\pi\pi}$ mass of the same quantities in the low $|t|$ region ($0.005 < |t| < 0.2$ GeV^2/c^2) is shown in figs. 10 and 11. (The mass bin $m_{\pi\pi} = 20$ MeV is used throughout the analysis.)

Not surprisingly, at low $|t|$ the helicity zero unnatural amplitudes g_0 and h_0 dominate the process, as would be expected for π exchange, while at high $|t|$ the two natural amplitudes g_N and h_N, which correspond to A_2 exchange, are strongest. However, the large difference in magnitude between g_0 and h_0 shows the incompleteness of the picture, as for π exchange (s-channel spin-flip only) the amplitudes with opposite nucleon transversity g_0 and h_0 should be equal. Analogous arguments hold for the S-wave, and we conclude that for both the S-wave and the P_0-wave nucleon helicity flip and non-flip amplitudes are simultaneously present. Consulting fig. 12, which shows the relation between helicity and transversity amplitudes, we conclude in addition that flip and non-flip amplitudes are out of phase.

If we interpret the process by means of one-particle exchange, we have to conclude that both unnatural exchanges, i.e. π exchange (s-channel nucleon helicity flip) and A_1 exchange (s-channel nucleon helicity non-flip), are contributing significantly to the process. The unnatural helicity-one P_U-wave, which was interpreted as being due to absorptive corrections to π exchange [16], also shows the difference between g_U and h_U, while according to Williams' "Poor man's absorption model" [17] only s-channel flip would be expected. This can be explained by the addition of A_1 exchange in the P_U-wave to the absorptive π exchange.

The natural parity exchange amplitudes g_N and h_N seem to agree at very low $|t|$ and also at high $|t|$ values, while for intermediate values of $|t|$ they differ strongly.

Contrary to π and A_1 exchange, A_2 exchange can contribute to both nucleon spin flip and non-flip amplitudes, but the s-channel non-flip amplitude is expected to be small [18] compared to the flip amplitude, and to be in phase [19] with it. Therefore the polarization in the natural parity exchange amplitudes (difference between g_N and h_N) seems to imply that an absorption effect also contributes here.

8. PARTIAL WAVE INTENSITIES AND ASYMMETRY

Although the information obtained in this experiment was insufficient for a unique determination of helicity amplitudes, we can still separate the intensities of the partial waves $|f|^2 + |n|^2 \equiv |h|^2 + |g|^2$ in a model-independent way. The results are shown in figs. 13 and 14 for the ρ mass region ($0.71 \leq m_{\pi\pi} \leq 0.83$ GeV/c^2) as a function of t and as a function of $m_{\pi\pi}$ for the low-t region ($0.005 < |t| < 0.2$ GeV^2/c^2). The fraction of natural parity exchange, as a function of t, rises from $\sim$ 10% at $|t| \sim m_\pi^2$ to $\sim$ 85% at $t \sim 1$ GeV^2/c^2 and falls slowly with increasing $m_{\pi\pi}$. This is in excellent agreement with an earlier analysis of hydrogen data based on positivity requirements for the density matrix [7].

In figs. 15 and 16 we show the asymmetry A separately for each partial wave. It is simply related to both helicity and also transversity amplitudes:

$$A = \frac{2\ \mathrm{Im}\ (nf^*)}{|n|^2 + |f|^2} = \pm \frac{|g|^2 - |h|^2}{|g|^2 + |h|^2}$$

with the negative sign for the natural partial wave.

The asymmetry of the unnatural partial waves decreases smoothly with increasing $m_{\pi\pi}$; as a function of t, the helicity-one wave drops quickly, compared with the rather constant helicity-zero wave. The asymmetry of the natural wave rises to a value close to -1 at $t \approx 0.2$ GeV^2/c^2 and drops to zero for large t.

9. RANK OF THE DENSITY MATRIX

It can generally be shown that by using suitable base vectors the density matrix for the unpolarized proton target can be split into two submatrices, one containing only terms with unnatural parity exchange amplitudes, the other with natural amplitudes [7,13,20]. Independently of the number of contributing amplitudes, both submatrices have at most rank (R) = 2. For the case of S and P waves only, with one natural parity exchange $\pi\pi$ partial wave, the rank satisfies $R \leq 3$. In an earlier analysis [7] making use of positivity constraints, it was found that at the ρ mass R = 2, while it was consistent with 2 for $m_{\pi\pi} < 900$ MeV. A necessary and sufficient condition for R = 2 is the proportionality of non-flip and flip amplitudes for unnatural parity exchange,

$$n = C\, f \ ,$$

with C the same complex constant for all unnatural amplitudes (C may depend on $m_{\pi\pi}$ and t). In particular, C = 0 also leads to R = 2, and the fact that the rank was found to be 2 was used as an argument supporting the assumed absence of A_1 exchange in earlier analyses. From the definitions of the amplitudes, it follows, with the above assumption, that

$$\frac{|g|}{|h|} = \frac{|C + i|}{|C - i|} \ .$$

This ratio is expected to be the same for all unnatural waves if R = 2, and to be unity if A_1 exchange is absent; fig. 17 shows it as a function of t, and fig. 18 as a function of $m_{\pi\pi}$ with the same cuts as previously. The ratio increases with mass consistent with $|C + i|/|C - i| = 0.54 + 1.20\ (m_{\pi\pi} - m_\rho)$, $(m_\rho = 0.77$ GeV), and the values for the S-wave tend to be somewhat higher (the numeric values have been obtained by a fit to the dominating P-wave). No significant dependence on t is seen; in the high-t region the $|g|/|h|$ ratio is badly determined owing to experimental errors.

The assumption that R = 2 for the density matrix leads to the complementary prediction that corresponding phases between unnatural transversity amplitudes are equal:

$$\gamma_{S0} = \chi_{S0} \; ; \quad \gamma_{U0} = \chi_{U0} \; .$$

This prediction seems to be compatible with our data in the ρ mass region, as a comparison with figs. 9 and 11 shows. However, for the "phase coherent" solution generally favoured by the $\pi^0\pi^0$ data indicated by ♦, we find a systematic discrepancy between γ_{S0} and χ_{S0} for $m_{\pi\pi}$ above the ρ mass region.

We conclude that we see a small deviation from the R = 2 assumption in the systematic difference between $|g_S|/|h_S|$ and $|g_0|/|h_0|$ as well as in the phases γ_{S0} and χ_{S0} above the ρ mass region.

10. A_1 EXCHANGE AND CONSEQUENCES FOR THE $\pi^+\pi^-$ PHASE-SHIFT ANALYSIS

One of the aims of this experiment was to check the assumptions on which previous $\pi^+\pi^-$ phase-shift analyses were based:

a) vanishing of the unnatural parity exchange s-channel helicity non-flip amplitudes, i.e. no A_1 exchange;

b) phase coherence: the s-channel flip amplitudes for the same exchange naturality and the same $\pi^+\pi^-$ spin are in phase.

Phase-shift analyses have been based either on the first [21] or on both [3,5,20,22] of these assumptions. The first of these assumptions is clearly violated, and we can establish a lower limit for the A_1 exchange amplitudes $|n| \geq 1/\sqrt{2}\,(\,||h| - |g||\,)$. This limit is reached when flip and non-flip amplitudes are 90° out of phase (n = Cf with C purely imaginary). The flip amplitude is then at its maximum, $|f| \leq 1/\sqrt{2}(|h| + |g|)$. The mass dependence of the lower limit of non-flip/flip amplitudes is given in fig. 19 for the low-t ($0.005 \leq |t| \leq 0.2$ GeV^2/c^2) region. For a determination of the magnitude of the A_1 exchange amplitude, one has to rely on a model fit [8,10,23] *).

*) From the fit in ref. 10, one finds for the P_0-wave non-flip/flip ratio a value of 35% in the ρ mass region at $|t| = m_\pi^2$.

In checking the second assumption (phase coherence), we encounter the difficulty that *a priori* the phases between the transversity amplitudes do not relate in a simple way to the phases between flip amplitudes, and the incomplete information from this experiment is insufficient to determine them. Only in the case of an R = 2 density matrix (n = C f), which is only approximately fulfilled, are the angles between flip amplitudes equal to the angles between transversity amplitudes, and the unknown phase between the set of g and the set of h amplitudes does not enter into the problem. Neglecting the R = 2 violation, we can therefore read directly, in figs. 9 and 11, the phases between amplitudes relevant for the phase-shift analysis. The mass dependence shows two distinct sets of solutions. For the solution indicated with ♦ the cosine of χ_{U0} is everywhere compatible with -1, whereas cos χ_{S0} is different from 1. This solution is in agreement with the assumption of phase coherence. The other solution (♢) shows the opposite behaviour with S-wave and helicity-zero P_0-wave in phase. Note that the ambiguity is only seen in the better-determined phases between the dominating h amplitudes. A similar ambiguity was already found in an earlier analysis [15] assuming the absence of A_1 exchange. In this analysis the second solution (the phase-coherent or "up" solution) was rejected because it leads to an S-wave structure with a width approximately equal to the width of the ρ. This is not observed in the $\pi^0\pi^0$ data.

In discussing the consequences of our findings on the old $\pi^+\pi^-$ phase-shift analysis, we assume that the s-channel nucleon helicity non-flip amplitude is due to A_1 exchange and not to a correction to π exchange which we assume to be given by the flip amplitude. Therefore only the flip amplitude should be extrapolated to the pole. If the rank condition were exactly fulfilled, the phases in the physical region determined in the old analysis would be identical while the magnitudes would be over-estimated by a factor $\sqrt{1 + |C|^2}$. This fact was pointed out by Ochs [24]. As mentioned before, we are still not able to determine C uniquely but can only give upper and lower limits. From the fit to the g_0/h_0 ratio, we obtain $0.30 < |C| < 3.4$, $1.04 < \sqrt{1 + |C|^2} < 3.6$ at the ρ mass. So in the case that |C| is close to the lower limit and that it shows a weak dependence on $m_{\pi\pi}$

and t (except at very low t, where it should increase strongly), the old phase shifts should be roughly correct. However, a new phase-shift analysis including the A_1 exchange contribution in the extrapolation procedure seems very desirable.

Acknowledgements

We have profited greatly from numerous discussions with R. Klanner, W. Ochs, M. Pennington and F. Wagner. In constructing the apparatus we were supported by Messrs. L. Bonet, H. Fischer and W. Mayr, as well as by the supporting staff at CERN and the MPI. Miss H. Carstens, Mrs. C. Ponting and Miss G. Waltermann assisted in data-taking and processing; Miss Waltermann contributed significantly to the computer program development. Special thanks are due to the Polarized Target Group at CERN, who supplied and maintained the target; in particular to Mr. J.M. Rieubland, who together with Mr. L. Mazzone developed the liquid-hydrogen target especially for us. Several of us wish to express their gratitude to CERN (K.R. and M.T.) and to the Max Planck Institute (J. de G., B.N., T.P. and M.T.) for their support and hospitality during the experiment.

REFERENCES

[1] G. Grayer et al., Nuclear Phys. B75 (1974) 189.

[2] A.B. Wicklund et al., Phys. Rev. D17 (1978) 1197.

[3] B. Hyams et al., Nuclear Phys. B64 (1973) 134.

[4] P. Estabrooks and A.D. Martin, Phys. Letters 53B (1974) 253.

[5] B. Hyams et al., Nuclear Phys. B100 (1975) 205.

[6] B. Hyams et al., Phys. Letters 51B (1974) 272.

[7] G. Grayer et al., Nuclear Phys. B50 (1972) 29.

[8] H. Becker et al., Proc. 18th Internat. Conf. on High-Energy Physics, Tbilisi, 1976 (JINR, Dubna, 1976), p. C27.

[9] H. Becker et al., Proc. 2nd Internat. Symp. on High-Energy Physics with Polarized Beams and Targets, Argonne, 1976 (American Institute of Physics, New York, 1976), p. 243.

[10] J.G.H. de Groot, Measurement of the reaction $\pi^- p \to \pi^-\pi^+ n$ at 17.2 GeV using a transversely polarized target, Thesis, University of Amsterdam (April 1978).

[11] G. Lutz and K. Rybicki, Nucleon polarization in the reaction $\pi^- p \to \pi^+\pi^- n$, MPI report MPI-PAE/Exp.EL.75 (October 1978).

[12] H. Becker et al., A model-independent partial wave analysis of the $\pi^+\pi^-$ system produced at low four-momentum transfer in the reaction $\pi^- p^\uparrow \to \pi^+\pi^- n$ at 17.2 GeV/c. Submitted to Nuclear Physics.

[13] B.R. Martin, D. Morgan and G. Shaw, Pion-pion interactions in particle physics (Academic Press, New York, 1976).
J.L. Petersen, CERN 77-04 (1977).

[14] W. de Boer, CERN 74-11 (1974).

[15] A cubic equation of the same form has been derived by P. Estabrooks and A.D. Martin, Phys. Letters 41B (1972) 350, assuming absence of A_1 exchange contributions.

[16] K. Gottfried and J.D. Jackson, Nuovo Cimento 34 (1964) 735.
F.S. Henyey et al., Phys. Rev. 182 (1969) 1579.

[17] P.K. Williams, Phys. Rev. D 1 (1970) 1312.
G.C. Fox, Proc. Conf. on Phenomenology in Particle Physics, Pasadena, 1971 (Calif. Inst. Tech., Pasadena, 1971), p. 703.

[18] B. Sadoulet, Nuclear Phys. B53 (1973) 135.

[19] J.D. Kimel and E. Reya, Proc. Internat. Conf. on $\pi\pi$ Scattering and Associated Topics, Tallahassee, 1973 (American Institute of Physics, New York, 1973), p. 274.

[20] W. Ochs, Nuovo Cimento 12A (1972) 724.

[21] P. Estabrooks and A.D. Martin, Phys. Letters 41B (1972) 350.

[22] W. Ochs, "Die Bestimmung von $\pi\pi$-Streuphasen auf der Grundlage einer Amplitudenanalyse der Reaktion $\pi^- p \to \pi^- \pi^+ n$ bei 17 GeV Primärimpuls", Thesis, Universität München (1973).

[23] J.D. Kimel and J.F. Owens, Nuclear Phys. B122 (1977) 464.

[24] W. Ochs, Proc. 2nd Internat. Conf. on Nucleon-Nucleon Interactions, Vancouver, 1977 (American Institute of Physics, New York, 1978), p. 326.

Table 1

Relations between moments and amplitudes

	"Helicity amplitudes" Non-spin flip: $n_S \equiv n_0^0$, $n_0 \equiv {}^U n_0^1$, $n_U \equiv {}^U n_1^1$, $n_N \equiv {}^N n_1^1$ Spin flip: $f_S \equiv f_0^0$, $f_0 \equiv {}^U f_0^1$, $f_U \equiv {}^U f_1^1$, $f_N \equiv {}^N f_1^1$	"Transversity amplitudes" Recoil transversity down: $g_S \equiv g_0^0$, $g_0 \equiv {}^U g_0^1$, $g_U \equiv {}^U g_1^1$, $g_N \equiv {}^N g_1^1$ Recoil transversity up: $h_S \equiv h_0^0$, $h_0 \equiv {}^U h_0^1$, $h_U \equiv {}^U h_1^1$, $h_N \equiv {}^N h_1^1$
$t_0^0 = (Y_0^0)$	$\frac{1}{\sqrt{4\pi}}(\lvert n_S\rvert^2 + \lvert f_S\rvert^2 + \lvert n_0\rvert^2 + \lvert f_0\rvert^2 + \lvert n_U\rvert^2 + \lvert f_U\rvert^2 + \lvert n_N\rvert^2 + \lvert f_N\rvert^2)$	$\frac{1}{\sqrt{4\pi}}(\lvert g_S\rvert^2 + \lvert h_S\rvert^2 + \lvert g_0\rvert^2 + \lvert h_0\rvert^2 + \lvert g_U\rvert^2 + \lvert h_U\rvert^2 + \lvert g_N\rvert^2 + \lvert h_N\rvert^2)$
$t_0^1 = (Y_0^1)$	$\frac{1}{\sqrt{\pi}}\,\mathrm{Re}\,(n_0 n_S^* + f_0 f_S^*)$	$\frac{1}{\sqrt{\pi}}\,\mathrm{Re}\,(g_0 g_S^* + h_0 h_S^*)$
$t_1^1 = 2(\mathrm{Re}\,Y_1^1)$	$\sqrt{\frac{2}{\pi}}\,\mathrm{Re}\,(n_U n_S^* + f_U f_S^*)$	$\sqrt{\frac{2}{\pi}}\,\mathrm{Re}\,(g_U g_S^* + h_U h_S^*)$
$t_0^2 = (Y_0^2)$	$\frac{1}{\sqrt{20\pi}}\left[2(\lvert n_0\rvert^2 + \lvert f_0\rvert^2) - \lvert n_U\rvert^2 - \lvert f_U\rvert^2 - \lvert n_N\rvert^2 - \lvert f_N\rvert^2\right]$	$\frac{1}{\sqrt{20\pi}}(2\lvert g_0\rvert^2 + 2\lvert h_0\rvert^2 - \lvert g_U\rvert^2 - \lvert h_U\rvert^2 - \lvert g_N\rvert^2 - \lvert h_N\rvert^2)$
$t_1^2 = 2(\mathrm{Re}\,Y_1^2)$	$\sqrt{\frac{6}{5\pi}}\,\mathrm{Re}\,(n_U n_0^* + f_U f_0^*)$	$\sqrt{\frac{6}{5\pi}}\,\mathrm{Re}\,(g_U g_0^* + h_U h_0^*)$
$t_2^2 = 2(\mathrm{Re}\,Y_2^2)$	$\sqrt{\frac{3}{10\pi}}(\lvert n_U\rvert^2 + \lvert f_U\rvert^2 - \lvert n_N\rvert^2 - \lvert f_N\rvert^2)$	$\sqrt{\frac{3}{10\pi}}(\lvert g_U\rvert^2 + \lvert h_U\rvert^2 - \lvert g_N\rvert^2 - \lvert h_N\rvert^2)$
$p_0^0 = 2(\cos\psi\, Y_0^0)$	$\frac{1}{\sqrt{4\pi}}\,2\,\mathrm{Im}\,(n_S f_S^* + n_0 f_0^* + n_U f_U^* + n_N f_N^*)$	$\frac{1}{\sqrt{4\pi}}(\lvert g_S\rvert^2 - \lvert h_S\rvert^2 + \lvert g_0\rvert^2 - \lvert h_0\rvert^2 + \lvert g_U\rvert^2 - \lvert h_U\rvert^2 - \lvert g_N\rvert^2 + \lvert h_N\rvert^2)$
$p_0^1 = 2(\cos\psi\, Y_0^1)$	$\frac{1}{\sqrt{\pi}}\,\mathrm{Im}\,(n_0 f_S^* - f_0 n_S^*)$	$\frac{1}{\sqrt{\pi}}\,\mathrm{Re}\,(g_0 g_S^* - h_0 h_S^*)$
$p_1^1 = 4(\cos\psi\,\mathrm{Re}\,Y_1^1)$	$\sqrt{\frac{2}{\pi}}\,\mathrm{Im}\,(n_U f_S^* - f_U n_S^*)$	$\sqrt{\frac{2}{\pi}}\,\mathrm{Re}\,(g_U g_S^* - h_U h_S^*)$
$p_0^2 = 2(\cos\psi\, Y_0^2)$	$\frac{1}{\sqrt{20\pi}}\,2\,\mathrm{Im}\,(2n_0 f_0^* - n_U f_U^* - n_N f_N^*)$	$\frac{1}{\sqrt{20\pi}}(2\lvert g_0\rvert^2 - 2\lvert h_0\rvert^2 - \lvert g_U\rvert^2 + \lvert h_U\rvert^2 + \lvert g_N\rvert^2 - \lvert h_N\rvert^2)$
$p_1^2 = 4(\cos\psi\,\mathrm{Re}\,Y_1^2)$	$\sqrt{\frac{6}{5\pi}}\,\mathrm{Im}\,(n_U f_0^* - f_U n_0^*)$	$\sqrt{\frac{6}{5\pi}}\,\mathrm{Re}\,(g_U g_0^* - h_U h_0^*)$
$p_2^2 = 4(\cos\psi\,\mathrm{Re}\,Y_2^2)$	$\sqrt{\frac{3}{10\pi}}\,2\,\mathrm{Im}\,(n_U f_U^* - n_N f_N^*)$	$\sqrt{\frac{3}{10\pi}}(\lvert g_U\rvert^2 - \lvert h_U\rvert^2 + \lvert g_N\rvert^2 - \lvert h_N\rvert^2)$
$r_1^1 = 4(\sin\psi\,\mathrm{Im}\,Y_1^1)$	$-\sqrt{\frac{2}{\pi}}\,\mathrm{Im}\,(n_N f_S^* + f_N n_S^*)$	$-\sqrt{\frac{2}{\pi}}\,\mathrm{Re}\,(g_N g_S^* - h_N h_S^*)$
$r_1^2 = 4(\sin\psi\,\mathrm{Im}\,Y_1^2)$	$-\sqrt{\frac{6}{5\pi}}\,\mathrm{Im}\,(n_N f_0^* + f_N n_0^*)$	$-\sqrt{\frac{6}{5\pi}}\,\mathrm{Re}\,(g_N g_0^* - h_N h_0^*)$
$r_2^2 = 4(\sin\psi\,\mathrm{Im}\,Y_2^2)$	$-\sqrt{\frac{6}{5\pi}}\,\mathrm{Im}\,(n_N f_U^* + f_N n_U^*)$	$-\sqrt{\frac{6}{5\pi}}\,\mathrm{Re}\,(g_N g_U^* - h_N h_U^*)$

Figure captions

Fig. 1 : Definition of kinematic quantities: ψ is the angle between the normal to the production plane and (transverse) polarization of the protons; θ, ϕ are the t-channel decay angles of the π^- in the rest frame of the $\pi\pi$ system.

Fig. 2 : Schematic view of the apparatus.

Fig. 3 : Missing-mass squared distribution for

a) events off butanol,

b) events from the hydrogen target,

c) product of left-right asymmetry and MM^2 distribution for events taken with the butanol target.

Fig. 4 : Distribution in the angle ψ of events for positive (full line) and for negative (broken line) target polarization. If no nucleon polarization effects were present, the two distributions would be identical.

Fig. 5 : Mass spectrum and normalized moments $\langle \mathrm{Re}\ Y_M^L \rangle$ for butanol.

Fig. 6 : Mass dependence (ΔM = 0.2 GeV) of cross-section (integrated over m-t bin), and normalized t-channel moments in the low-t region ($0.005 < |t| < 0.2$ GeV$^2/c^2$) scaled to 100% polarized protons.

Fig. 7 : t-dependence of cross-section and normalized t-channel moments in the ρ region ($0.71 < m_{\pi\pi} < 0.83$ GeV/c^2) scaled to 100% polarized protons.

Fig. 8 : t-dependence of the moduli of the transversity amplitudes ($0.71 < < m_{\pi\pi} < 0.83$ GeV/c^2). The amplitudes are normalized so that their squares add up to unity.

Fig. 9 : Cosines of the phases between transversity amplitudes corresponding to unnatural parity exchange.

Fig. 10 : Mass dependence of the moduli of the transversity amplitudes ($0.005 < |t| < 0.2$ GeV$^2/c^2$). Normalization as in Fig. 8.

Fig. 11 : Mass dependence of the cosines of the phases between transversity amplitudes ($0.005 < |t| < 0.2$ GeV$^2/c^2$).

Fig. 12 : Relation between helicity and transversity amplitudes:
a) general case,
b) phase coherence between flip and non-flip amplitudes.

Fig. 13 : t-dependence of the normalized partial wave intensities ($0.71 < m_{\pi\pi} < 0.83$ GeV/c^2).

Fig. 14 : Mass dependence of a) normalized and b) unnormalized partial wave intensities ($0.005 < |t| < 0.2$ GeV$^2/c^2$).

Fig. 15 : t-dependence of the asymmetries of the partial waves ($0.71 < m_{\pi\pi} < 0.83$ GeV/c^2).

Fig. 16 : Mass dependence of the asymmetries ($0.005 < |t| < 0.2$ GeV$^2/c^2$).

Fig. 17 : t-dependence of the ratios $|g|/|h|$ for the unnatural partial waves ($0.71 < m_{\pi\pi} < 0.83$ GeV/c^2).

Fig. 18 : Mass dependence of the ratios $|g|/|h|$ for the unnatural partial waves ($0.005 < |t| < 0.2$ GeV$^2/c^2$).

Fig. 19 : Minimum ratio between non-flip and flip amplitudes for the unnatural parity exchange partial waves ($0.005 < |t| < 0.2$ GeV$^2/c^2$).

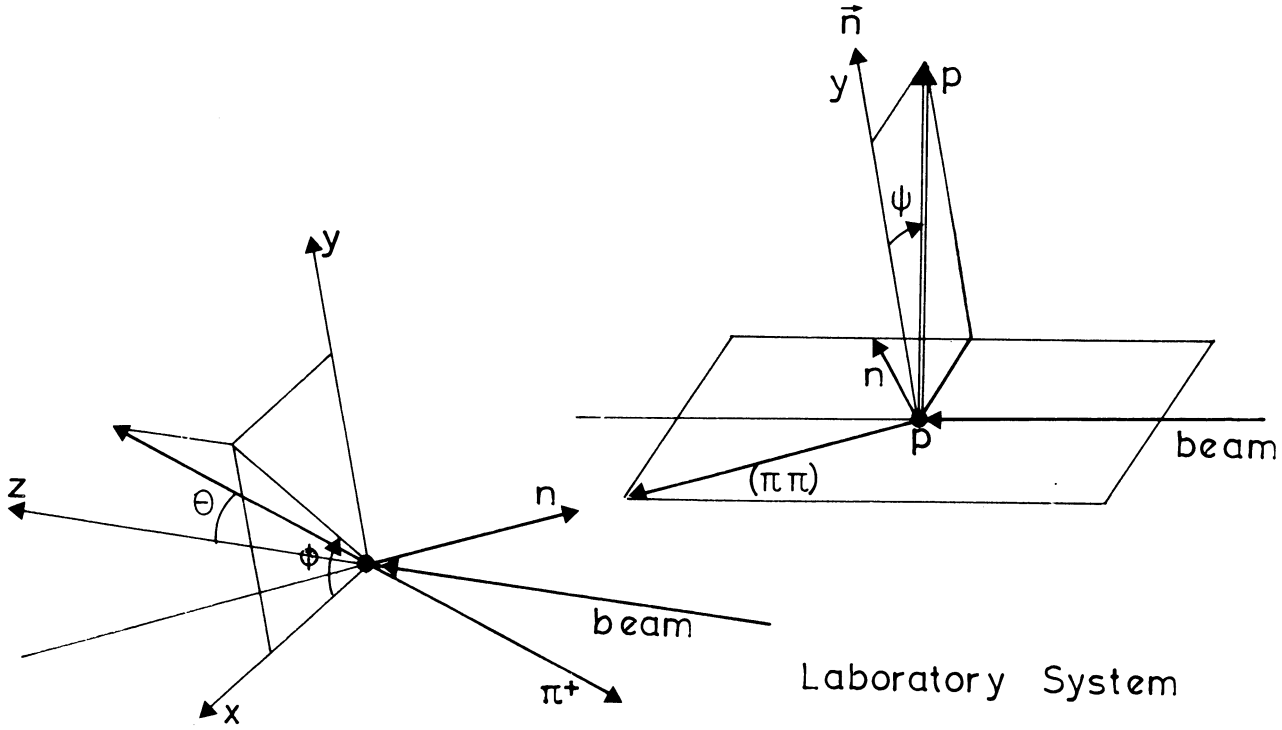
$\vec{n}$
y
p
ψ
n
p
beam
(ππ)
Laboratory System
y
z
Θ
Φ
n
beam
π+
x
Rest System of (π+π−)

Fig. 1

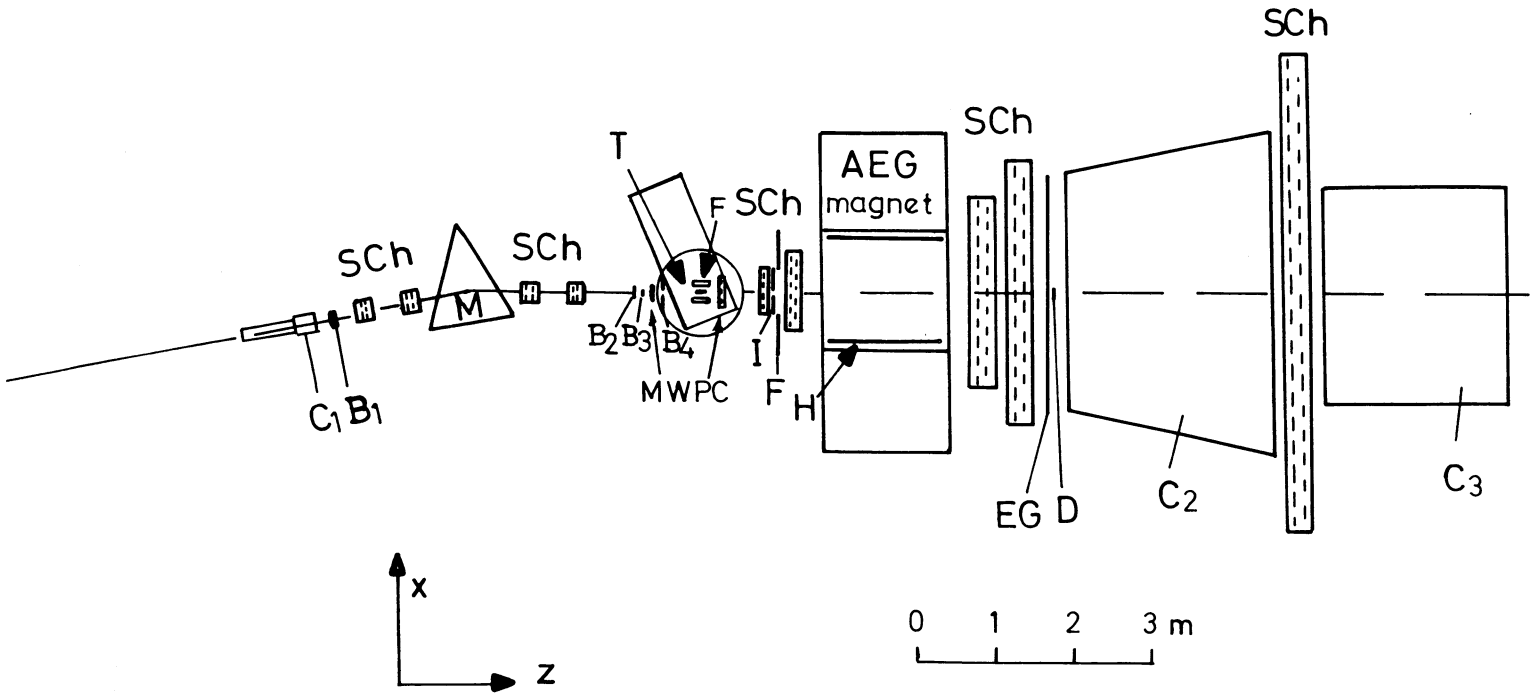
SCh
SCh
M
T
F
SCh
AEG
magnet
SCh
SCh
B_2 B_3 B_4
MWPC
I
F
H
C_1 B_1
EG
D
C_2
C_3
x
z
0 1 2 3 m

Fig. 2

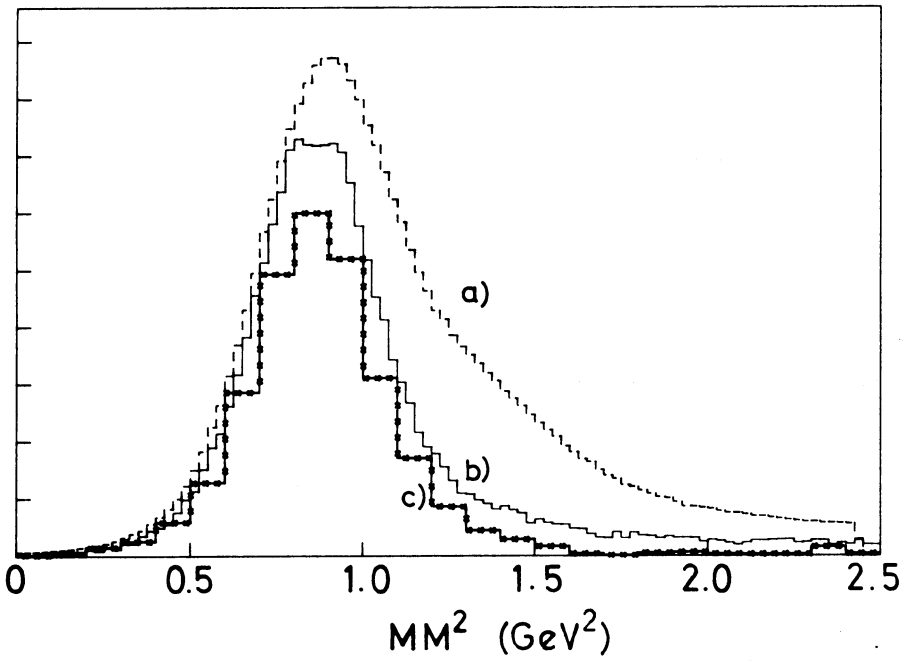
a)
b)
c)
0
0.5
1.0
1.5
2.0
2.5
MM² (GeV²)

Fig. 3

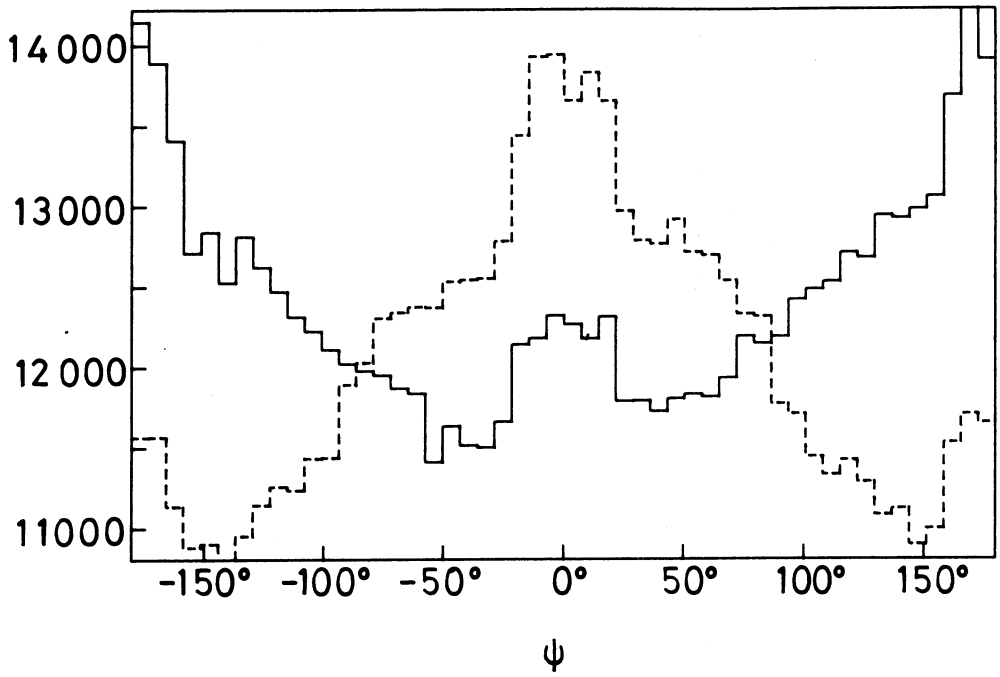
14 000
13000
12 000
11000
-150°
-100°
-50°
0°
50°
100°
150°
ψ

Fig. 4

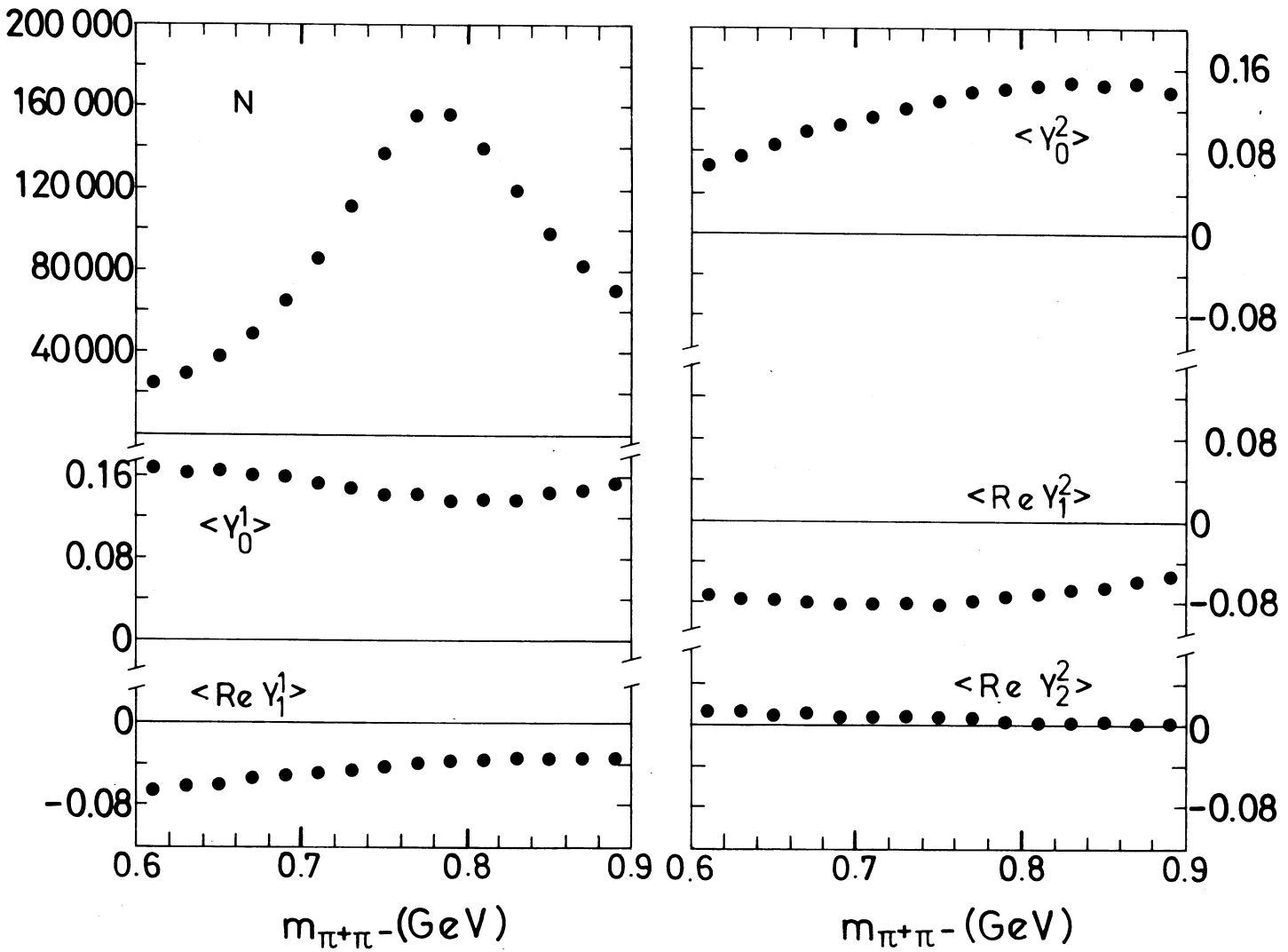
200 000
160 000
120 000
80000
40000
N
0.16
0.08
0
$\langle Y_0^1 \rangle$
0
$\langle Re\ Y_1^1 \rangle$
-0.08
0.6
0.7
0.8
0.9
$m_{\pi^+\pi^-}$-(GeV)
0.16
0.08
0
-0.08
$\langle Y_0^2 \rangle$
0.08
0
-0.08
$\langle Re\ Y_1^2 \rangle$
0
-0.08
$\langle Re\ Y_2^2 \rangle$
0.6
0.7
0.8
0.9
$m_{\pi^+\pi^-}$-(GeV)

Fig. 5

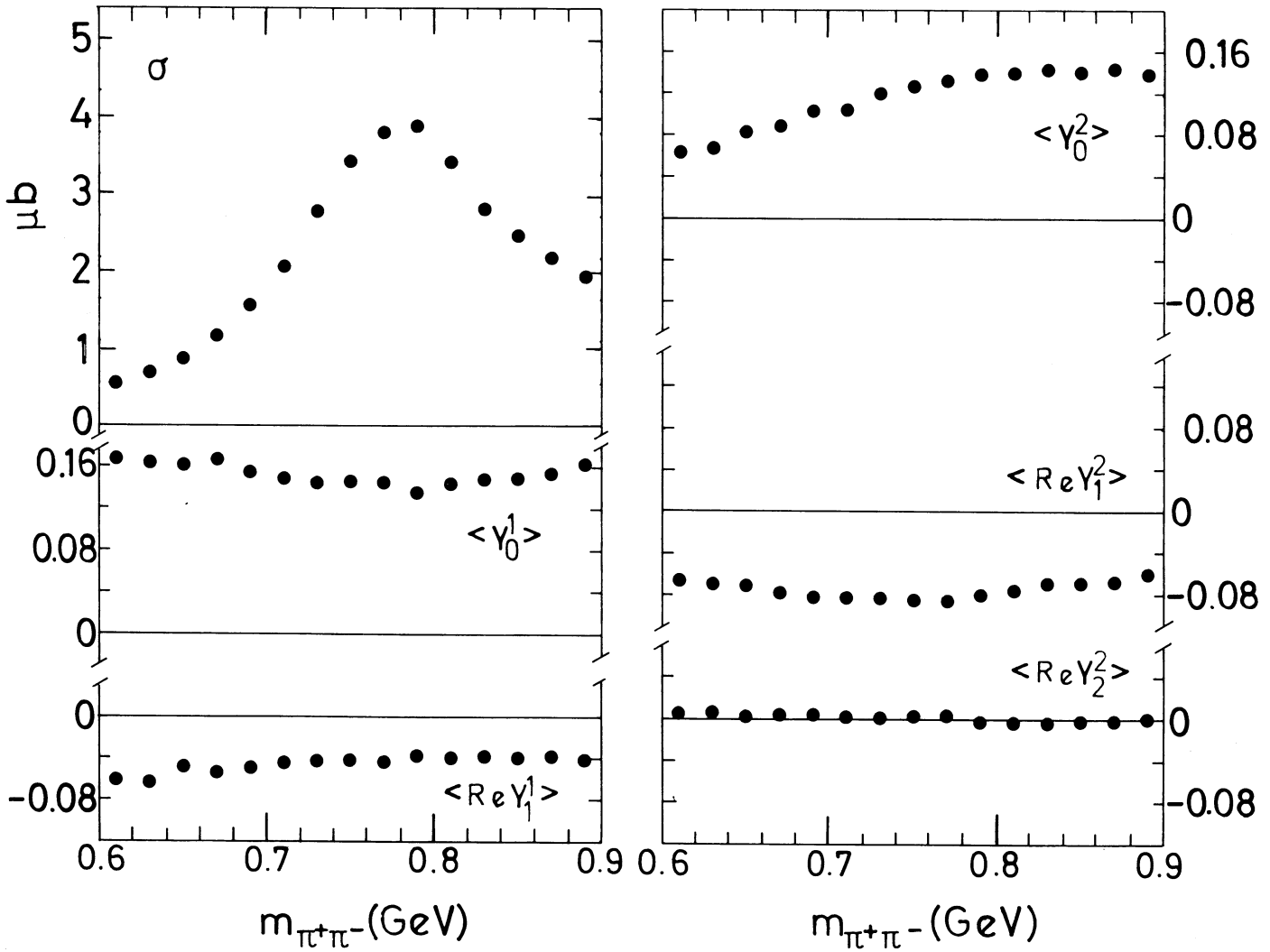
σ
μb
5
4
3
2
1
0
0.16
0.08
0
-0.08
$\langle Y_0^1 \rangle$
$\langle Re Y_1^1 \rangle$
$\langle Y_0^2 \rangle$
$\langle Re Y_1^2 \rangle$
$\langle Re Y_2^2 \rangle$
0.6
0.7
0.8
0.9
$m_{\pi^+\pi^-}$-(GeV)

Fig. 6a

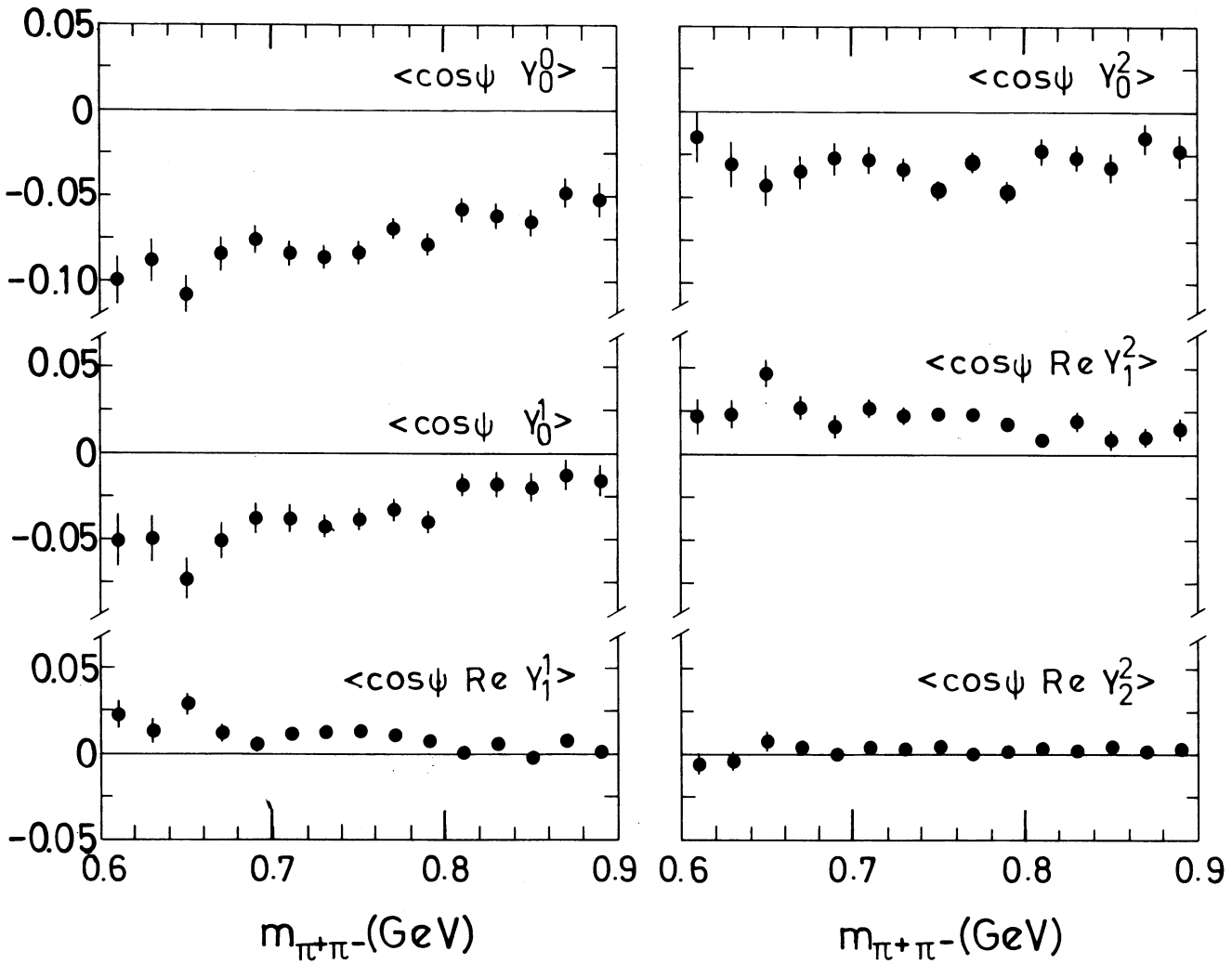
0.05
0
-0.05
-0.10
<cosψ Y_0^0>
<cosψ Y_0^2>
0.05
0
-0.05
<cosψ Y_0^1>
<cosψ Re Y_1^2>
0.05
0
-0.05
<cosψ Re Y_1^1>
<cosψ Re Y_2^2>
0.6
0.7
0.8
0.9
$m_{\pi^+\pi^-}$(GeV)
$m_{\pi^+\pi^-}$(GeV)

Fig. 6b

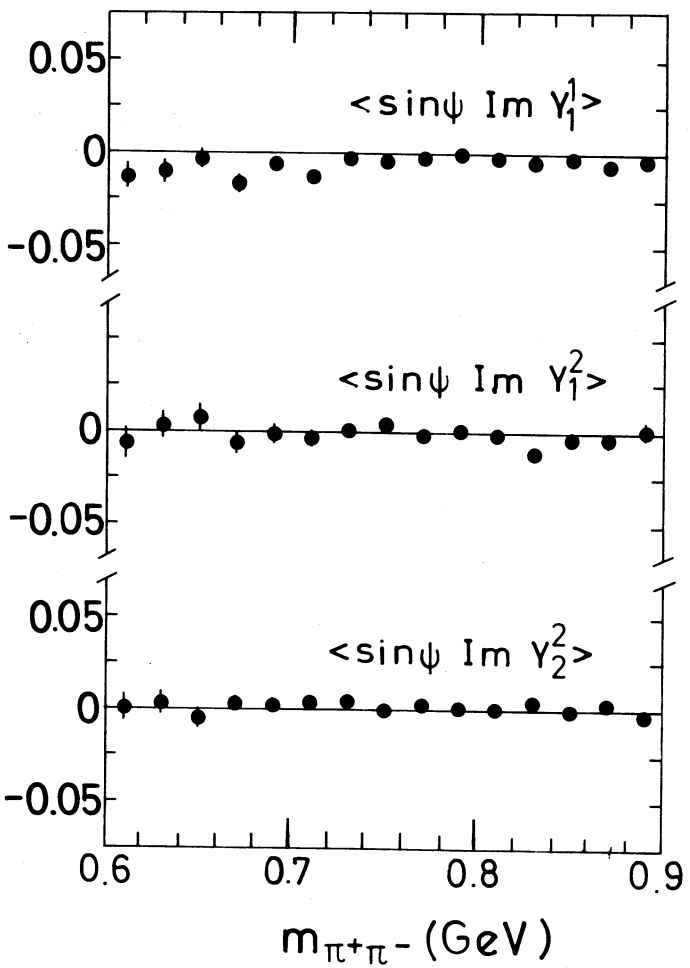
0.05
0
-0.05
<sinψ Im Y$_1^1$>
<sinψ Im Y$_1^2$>
<sinψ Im Y$_2^2$>
0.6
0.7
0.8
0.9
$m_{\pi^+\pi^-}$ (GeV)

Fig. 6c

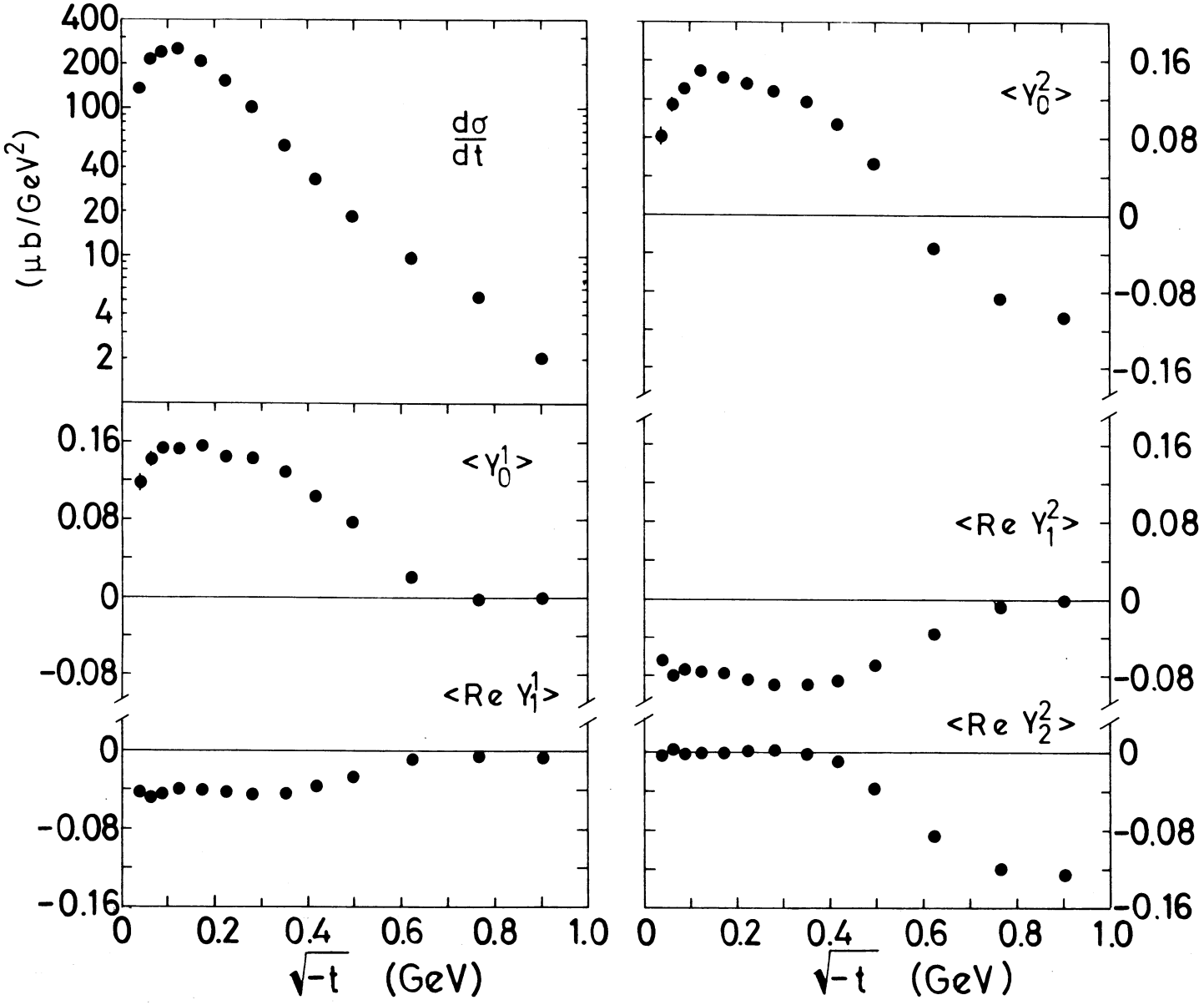
400
200
100
40
20
10
4
2
(μb/GeV²)
dσ/dt
<Y₀¹>
<Re Y₁¹>
<Y₀²>
<Re Y₁²>
<Re Y₂²>
0.16
0.08
0
-0.08
-0.16
0
0.2
0.4
0.6
0.8
1.0
√-t (GeV)

Fig. 7a

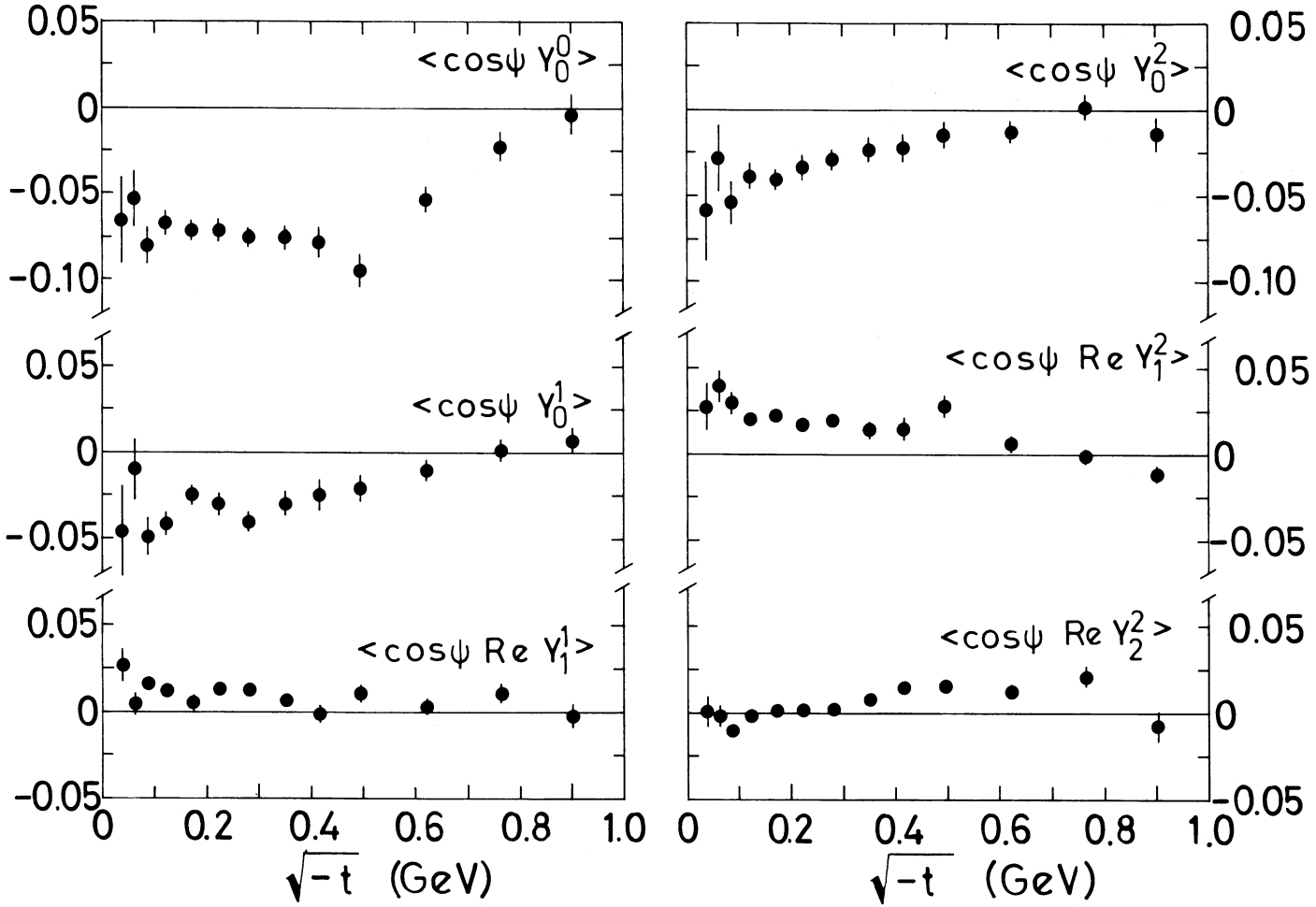
0.05
0
-0.05
-0.10
<cosψ Y_0^0>
<cosψ Y_0^2>
<cosψ Y_0^1>
<cosψ Re Y_1^2>
<cosψ Re Y_1^1>
<cosψ Re Y_2^2>
0
0.2
0.4
0.6
0.8
1.0
$\sqrt{-t}$ (GeV)

Fig. 7b

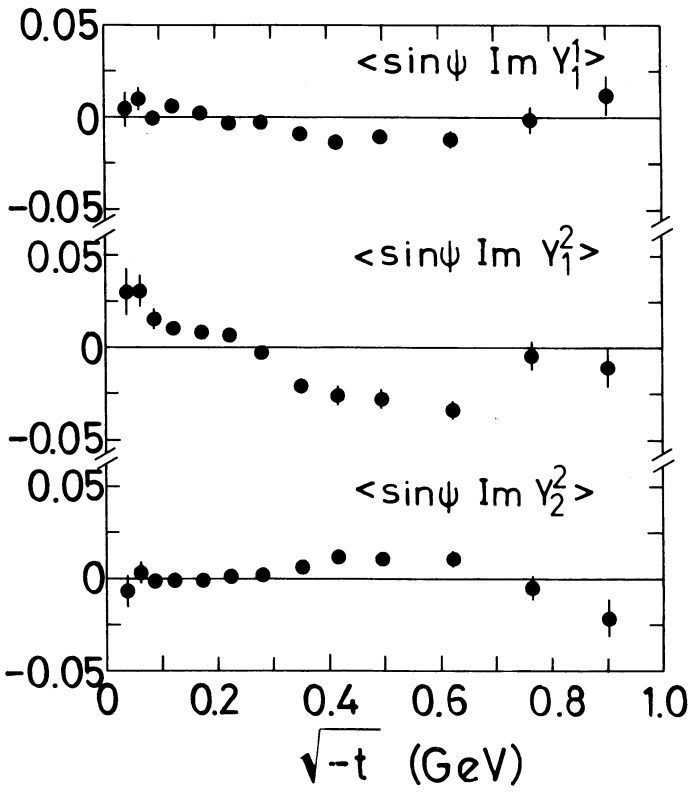
0.05
0
-0.05
<sinψ Im Y$_1^1$>
0.05
0
-0.05
<sinψ Im Y$_1^2$>
0.05
0
-0.05
<sinψ Im Y$_2^2$>
0
0.2
0.4
0.6
0.8
1.0
$\sqrt{-t}$ (GeV)

Fig. 7c

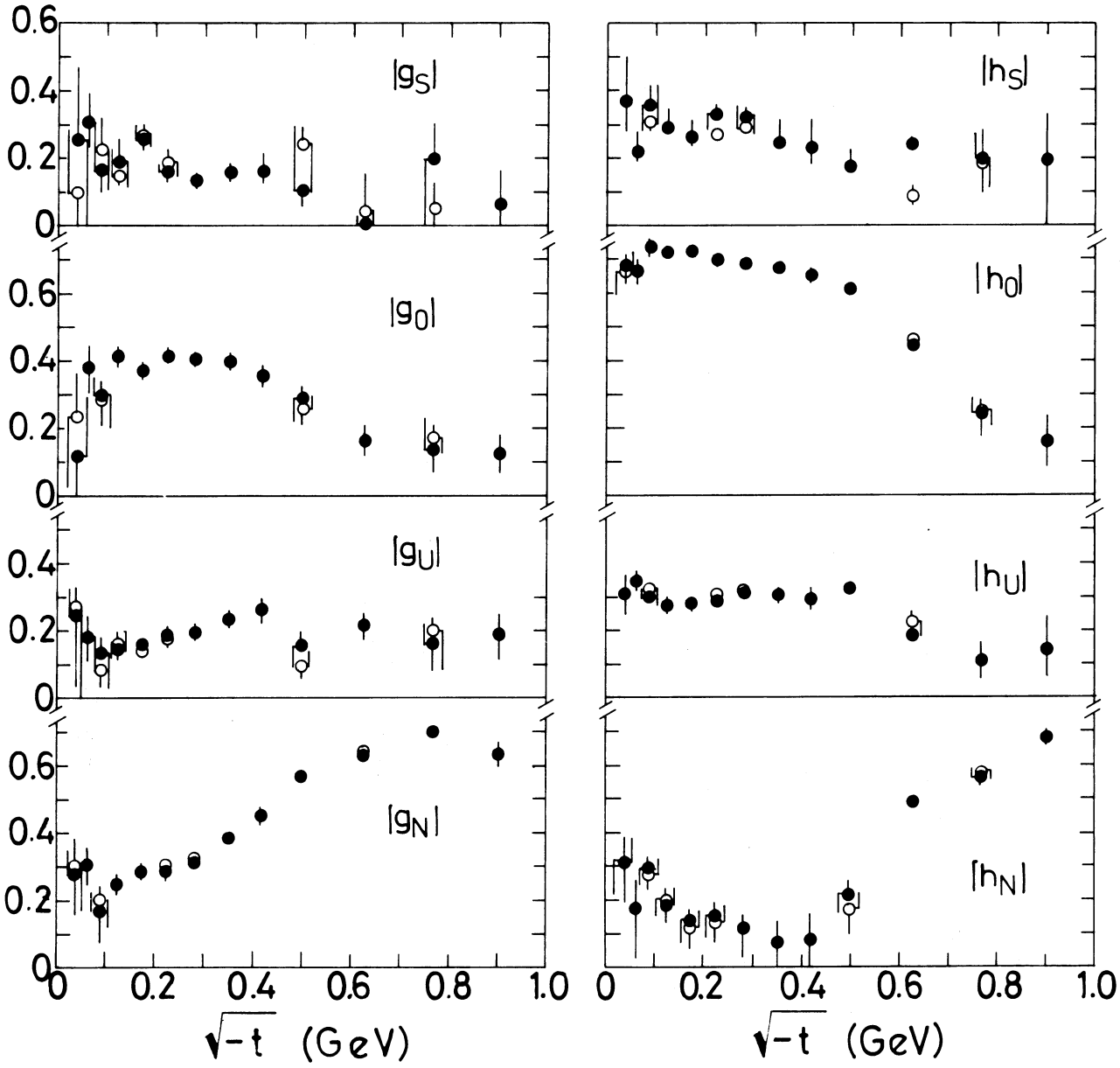

Fig. 8

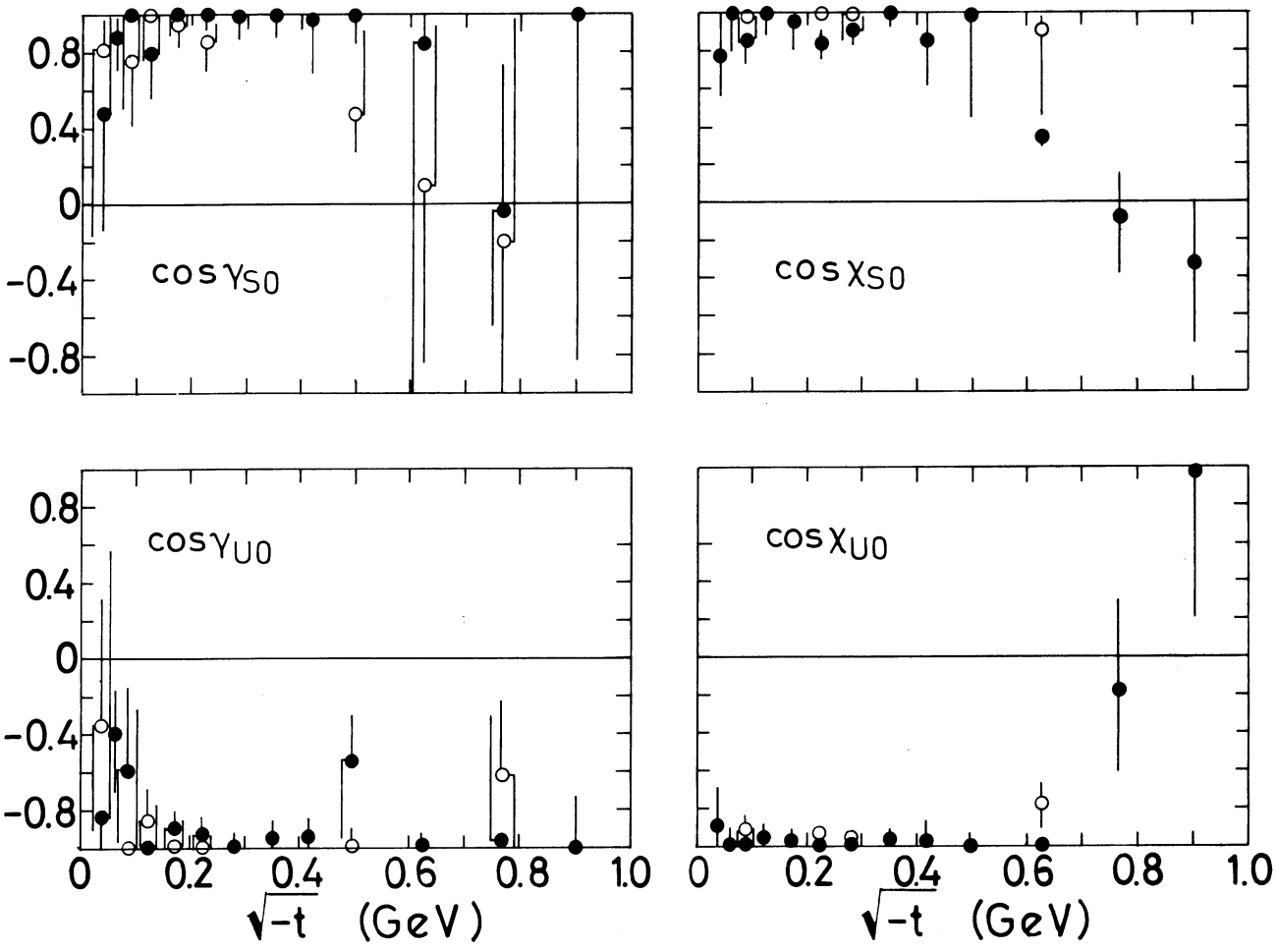

Fig. 9

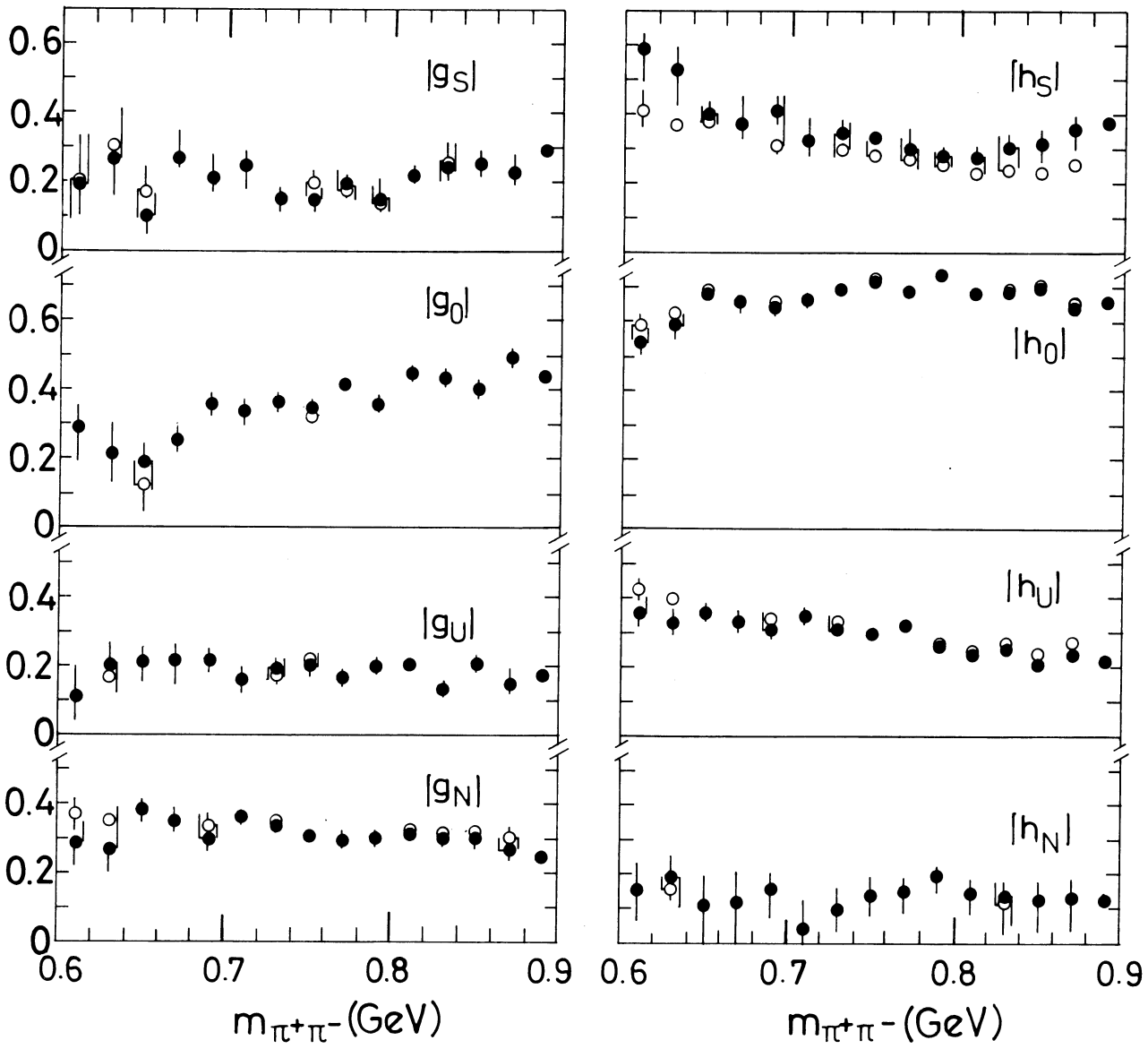

Fig. 10

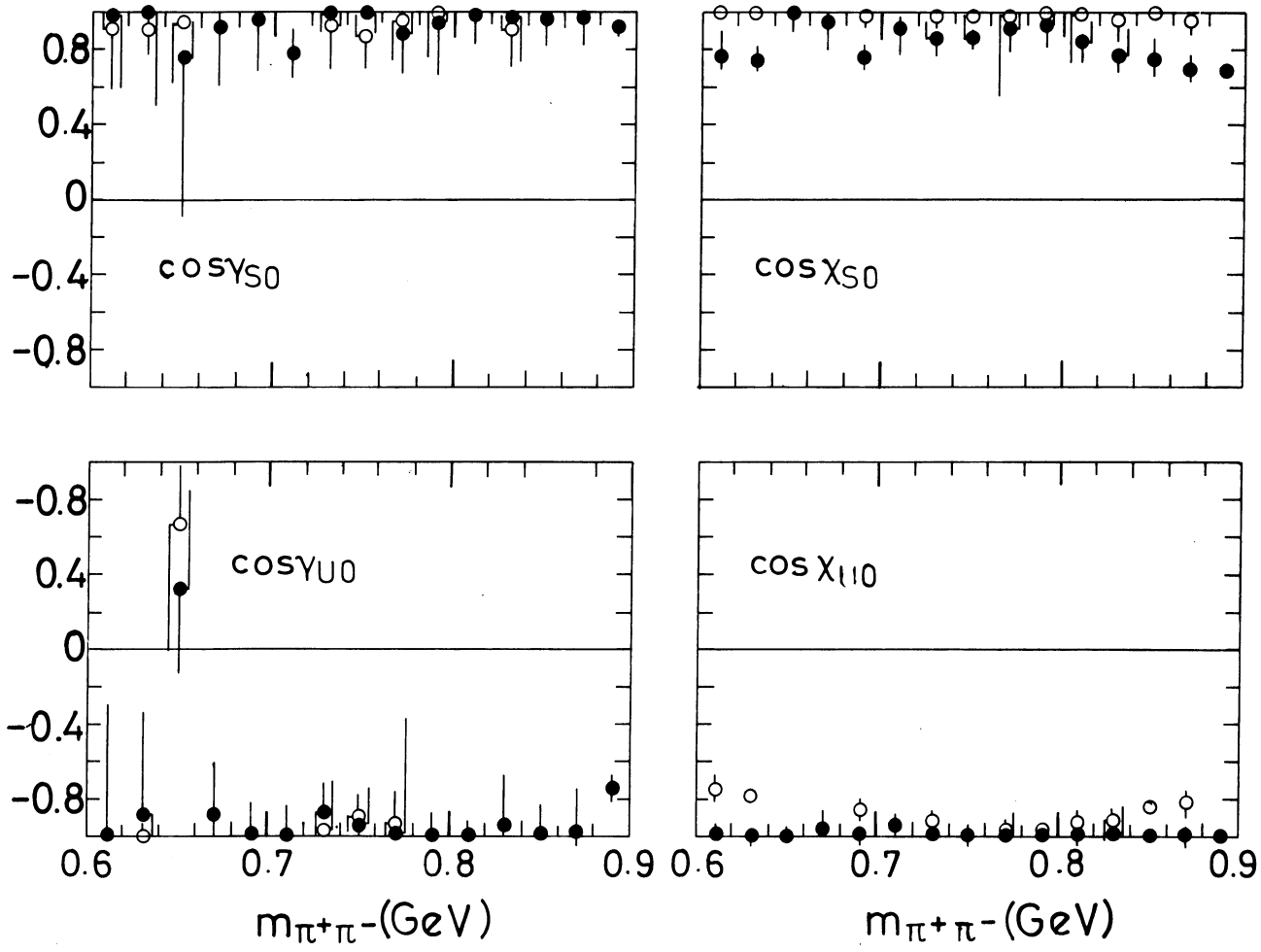
0.8
0.4
0
-0.4
-0.8
cosγS0
cosχS0
cosγU0
cosχL10
0.6
0.7
0.8
0.9
mπ+π-(GeV)
mπ+π-(GeV)

Fig. 11

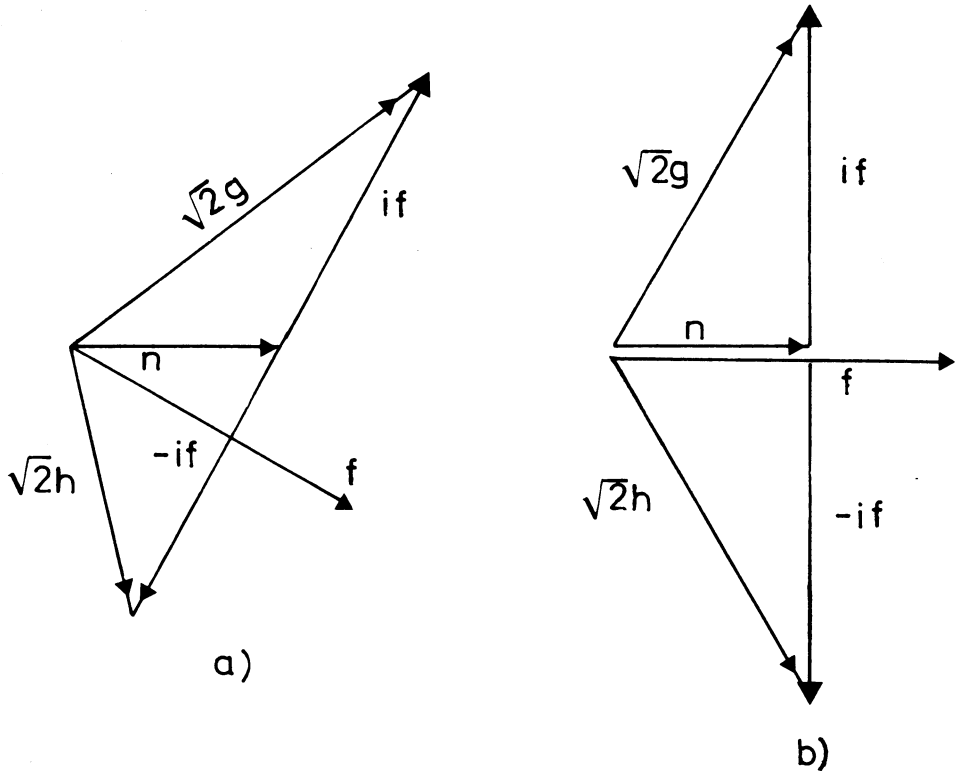

Fig. 12

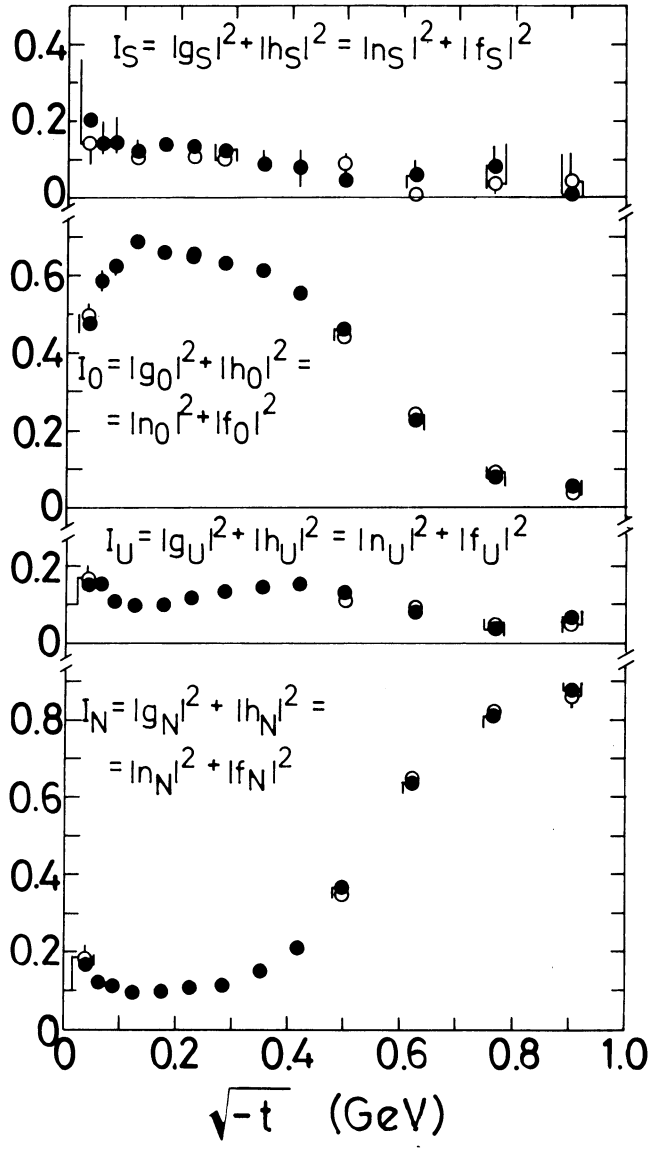
$I_S = |g_S|^2 + |h_S|^2 = |n_S|^2 + |f_S|^2$
$I_0 = |g_0|^2 + |h_0|^2 =$
$= |n_0|^2 + |f_0|^2$
$I_U = |g_U|^2 + |h_U|^2 = |n_U|^2 + |f_U|^2$
$I_N = |g_N|^2 + |h_N|^2 =$
$= |n_N|^2 + |f_N|^2$
0.4
0.2
0
0.6
0.4
0.2
0
0.2
0
0.8
0.6
0.4
0.2
0
0
0.2
0.4
0.6
0.8
1.0
$\sqrt{-t}$ (GeV)

Fig. 13

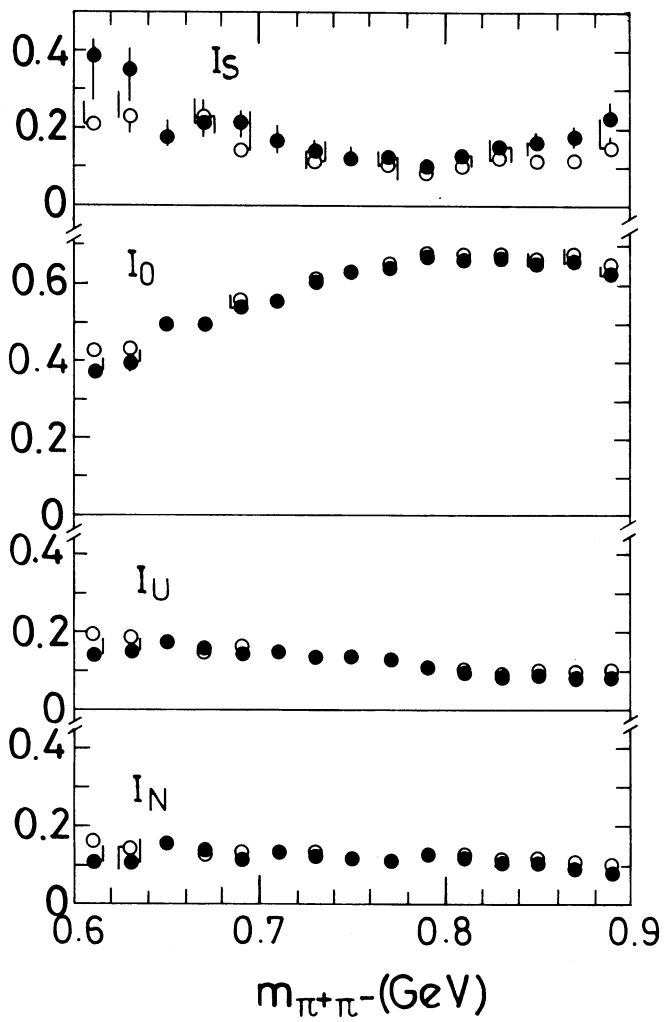
0.4
0.2
0
I_S
0.6
0.4
0.2
0
I_0
0.4
0.2
0
I_U
0.4
0.2
0
I_N
0.6
0.7
0.8
0.9
$m_{\pi^+\pi^-}$-(GeV)

a)

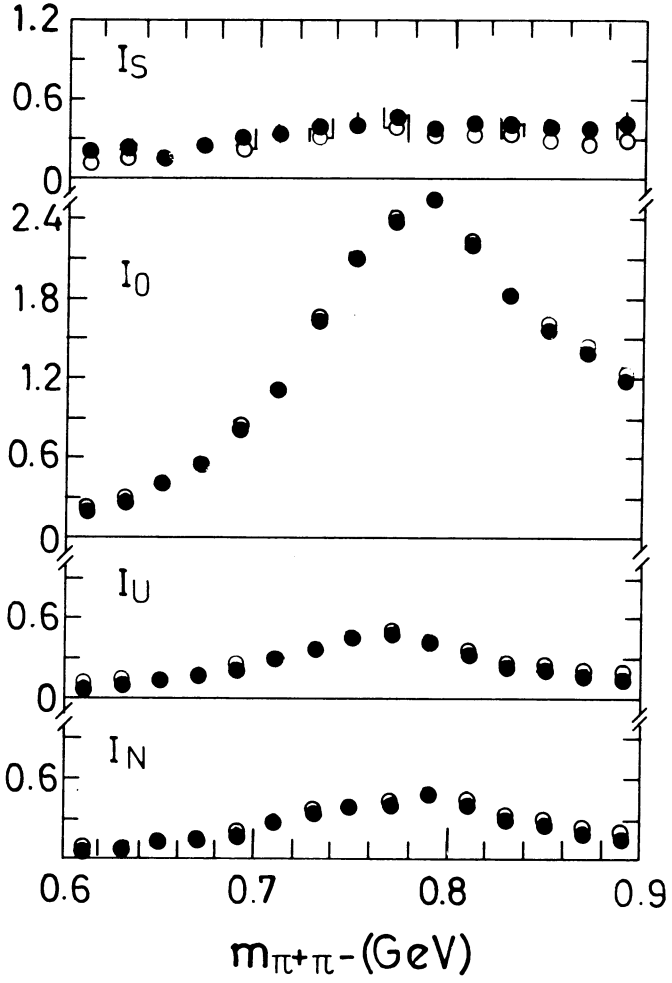
1.2
0.6
0
I_S
2.4
1.8
1.2
0.6
0
I_0
0.6
0
I_U
0.6
I_N
0.6
0.7
0.8
0.9
$m_{\pi^+\pi^-}$-(GeV)

b)

Fig. 14

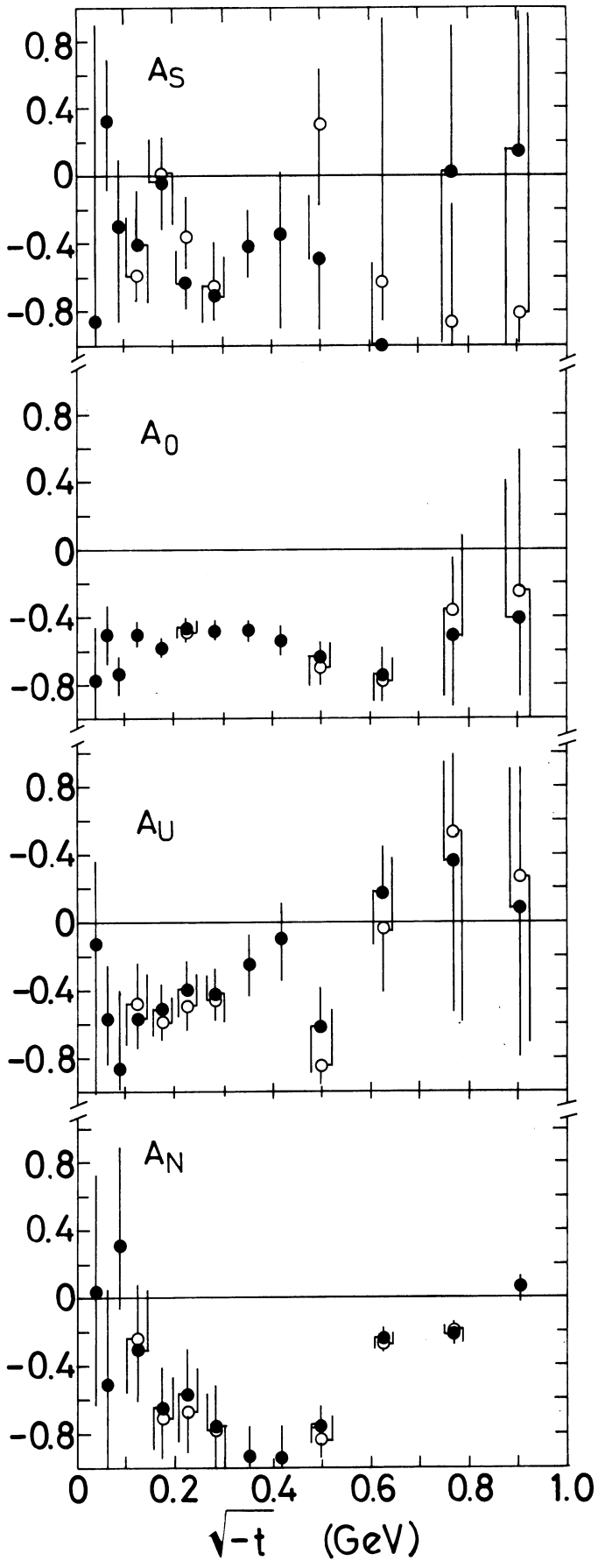

Fig. 15

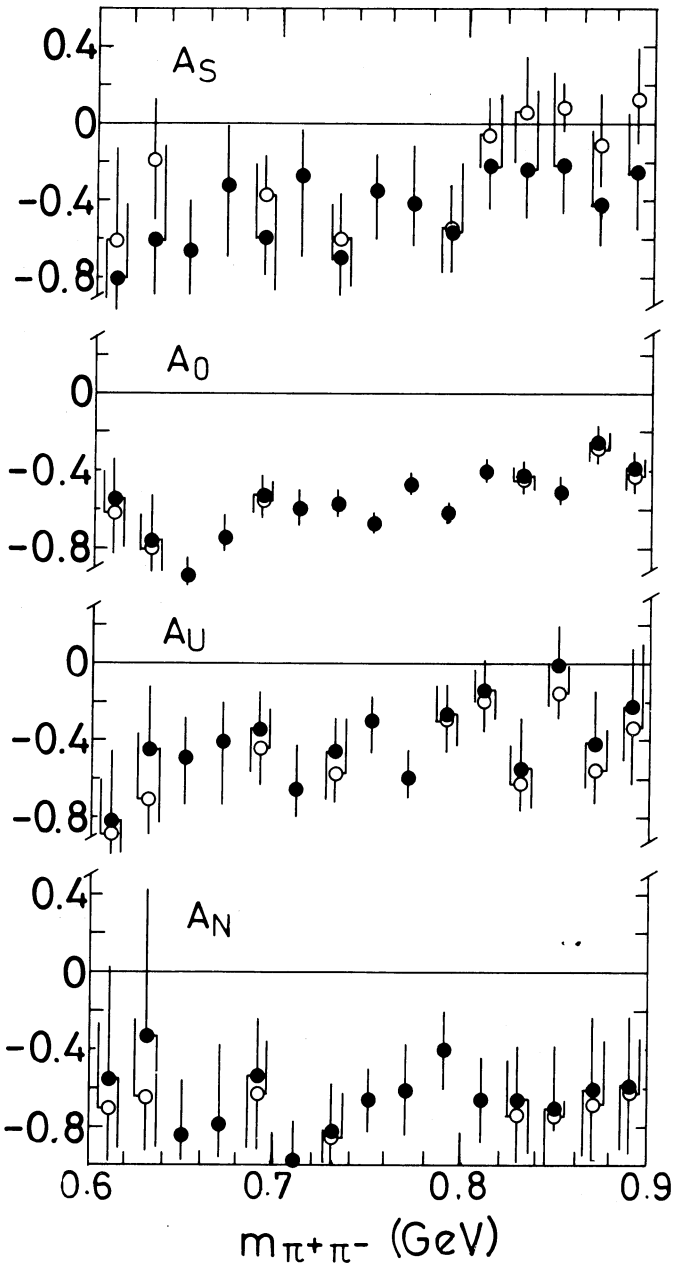

Fig. 16

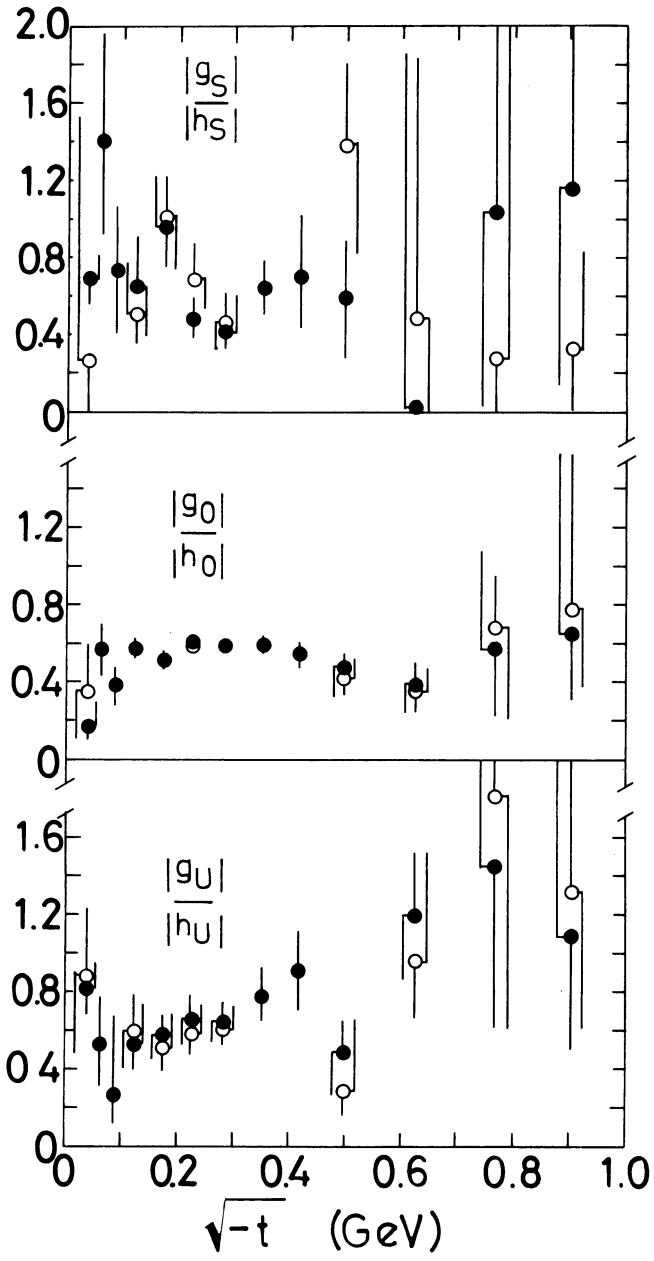
2.0
1.6
1.2
0.8
0.4
0
$\frac{|g_S|}{|h_S|}$
1.2
0.8
0.4
0
$\frac{|g_0|}{|h_0|}$
1.6
1.2
0.8
0 4
0
$\frac{|g_U|}{|h_U|}$
0
0.2
0.4
0.6
0.8
1.0
$\sqrt{-t}$ (GeV)

Fig. 17

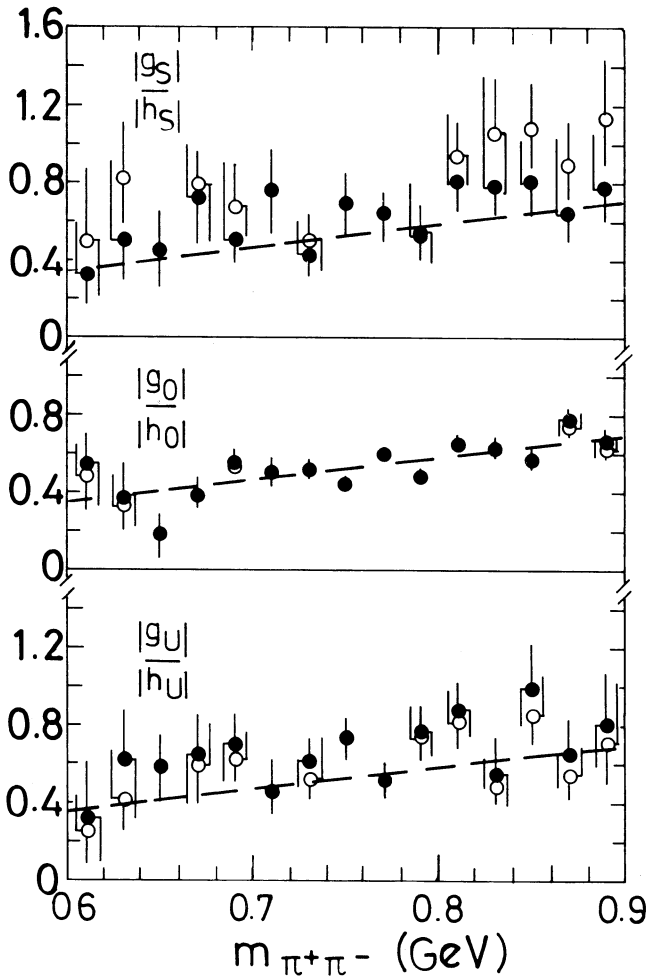
1.6
1.2
0.8
0.4
0
$\left|\frac{g_S}{h_S}\right|$
$\left|\frac{g_0}{h_0}\right|$
$\left|\frac{g_U}{h_U}\right|$
0.6
0.7
0.8
0.9
$m_{\pi^+\pi^-}$ (GeV)

Fig. 18

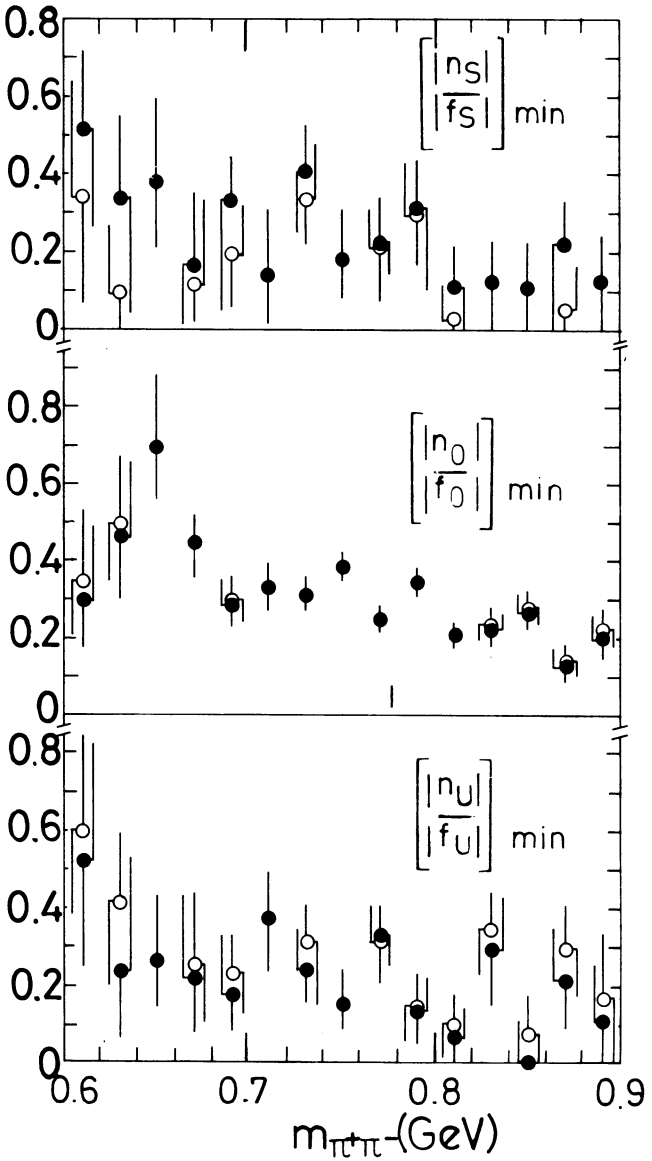
0.8
0.6
0.4
0.2
0
$\left[\frac{|n_S|}{|f_S|}\right]_{min}$
$\left[\frac{|n_0|}{|f_0|}\right]_{min}$
$\left[\frac{|n_U|}{|f_U|}\right]_{min}$
0.6
0.7
0.8
0.9
$m_{\pi^+\pi^-}$(GeV)

Fig. 19